NeuroImage 226 (2021) 117590

Contents lists available at ScienceDirect

NeuroImage

journal homepage: www.elsevier.com/locate/neuroimage

Cholinergic and dopaminergic effects on prediction error and uncertainty responses during sensory associative learning

Sandra Iglesias[a,*], Lars Kasper[a,b], Samuel J. Harrison[a], Robert Manka[c], Christoph Mathys[a,d], Klaas E. Stephan[a,e]

[a] Translational Neuromodeling Unit (TNU), Institute for Biomedical Engineering, University of Zurich & Swiss Federal Institute of Technology (ETH Zurich), Wilfriedstr. 6, 8032 Zurich, Switzerland
[b] Institute for Biomedical Engineering, ETH Zurich and University of Zurich, Switzerland
[c] Department of Cardiology, University Hospital Zurich, Switzerland
[d] Interacting Minds Centre, Aarhus University, Aarhus, Denmark
[e] Max Planck Institute for Metabolism Research, Cologne, Germany

ARTICLE INFO

Keywords:
Acetylcholine
Dopamine
Biperiden
Amisulpride
Basal forebrain
Ventral tegmental area
Substantia nigra
Neuromodulation
fMRI
Hierarchical Gaussian Filter

ABSTRACT

Navigating the physical world requires learning probabilistic associations between sensory events and their change in time (volatility). Bayesian accounts of this learning process rest on hierarchical prediction errors (PEs) that are weighted by estimates of uncertainty (or its inverse, precision). In a previous fMRI study we found that low-level precision-weighted PEs about visual outcomes (that update beliefs about associations) activated the putative dopaminergic midbrain; by contrast, precision-weighted PEs about cue-outcome associations (that update beliefs about volatility) activated the cholinergic basal forebrain. These findings suggested selective dopaminergic and cholinergic influences on precision-weighted PEs at different hierarchical levels.

Here, we tested this hypothesis, repeating our fMRI study under pharmacological manipulations in healthy participants. Specifically, we performed two pharmacological fMRI studies with a between-subject double-blind placebo-controlled design: study 1 used antagonists of dopaminergic (amisulpride) and muscarinic (biperiden) receptors, study 2 used enhancing drugs of dopaminergic (levodopa) and cholinergic (galantamine) modulation.

Pooled across all pharmacological conditions of study 1 and study 2, respectively, we found that low-level precision-weighted PEs activated the midbrain and high-level precision-weighted PEs the basal forebrain as in our previous study. However, we found pharmacological effects on brain activity associated with these computational quantities only when splitting the precision-weighted PEs into their PE and precision components: in a brainstem region putatively containing cholinergic (pedunculopontine and laterodorsal tegmental) nuclei, biperiden (compared to placebo) enhanced low-level PE responses and attenuated high-level PE activity, while amisulpride reduced high-level PE responses. Additionally, in the putative dopaminergic midbrain, galantamine compared to placebo enhanced low-level PE responses (in a body-weight dependent manner) and amisulpride enhanced high-level precision activity. Task behaviour was not affected by any of the drugs.

These results do not support our hypothesis of a clear-cut dichotomy between different hierarchical inference levels and neurotransmitter systems, but suggest a more complex interaction between these neuromodulatory systems and hierarchical Bayesian quantities. However, our present results may have been affected by confounds inherent to pharmacological fMRI. We discuss these confounds and outline improved experimental tests for the future.

1. Introduction

Navigating complex physical environments requires a representation of probabilistic associations between events in the world. A popular notion in contemporary computational and cognitive neuroscience is that the brain masters this challenge by constructing and continuously updating an internal model of the environment (technically speaking, a generative model of its sensory inputs; Dayan et al., 1995; Friston, 2005). This generative model then serves to infer the hidden causes of current sensations and predict future sensations.

* Corresponding author.
E-mail address: iglesias@biomed.ee.ethz.ch (S. Iglesias).

https://doi.org/10.1016/j.neuroimage.2020.117590
Received 6 June 2020; Received in revised form 20 October 2020; Accepted 19 November 2020
Available online 4 December 2020

This general "Bayesian brain" notion is reflected by several concrete concepts, such as predictive coding (Rao and Ballard, 1999; Friston, 2005) or hierarchical filtering (Mathys et al., 2011). In accordance with long-standing neuroanatomical findings (Felleman and Van Essen, 1991; Hilgetag et al., 2000), these concepts assume that the brain's model has a hierarchical structure, providing a basis for hierarchical Bayesian inference. Put simply, the key idea is that each level of the hierarchy holds a belief or prediction about the level below that is updated by ascending prediction errors (PEs).

One established experimental paradigm to probe hierarchical inference is probabilistic associative learning under volatility. This involves cue-outcome pairs whose association strengths change over time (Behrens et al., 2007; Iglesias et al., 2013; Diaconescu et al., 2017). In this setting, the brain needs to compute two different types of PEs for updating hierarchically coupled beliefs: a low-level PE about the outcome and a high-level PE about the probability of that outcome. Importantly, these PEs are weighted by estimates of uncertainty (or precision, the inverse of uncertainty) that modulate the magnitude of belief updates (Mathys et al., 2011; Mathys et al., 2014).

We have previously established an associative sensory learning task under volatility which is tailored to analysis by a hierarchical Bayesian model (Iglesias et al., 2013). A functional magnetic resonance imaging (fMRI) study of this task in healthy volunteers suggested a possible link between different precision-weighted PEs and activity in distinct neuromodulatory regions. In brief, we found that low-level precision-weighted PEs about sensory outcome (ε_2) activated the putative dopaminergic midbrain, whereas high-level precision-weighted PEs about the outcome's probability (ε_3) were reflected by activity in the cholinergic basal forebrain, or more precisely, in its septal subregion (area Ch1-2; Zaborszky et al., 2008). A subsequent study using a similar computational model replicated these effects for social learning, with low-level PEs activating the putative dopaminergic midbrain and high-level PEs activating the basal forebrain (Diaconescu et al., 2017).

The possibility that activity of two distinct neuromodulatory systems could be probed by a single neuroimaging paradigm is intriguing, given the need for computational assays of neuromodulation that could guide differential diagnosis and treatment prediction in psychiatry (Stephan et al., 2006; Stephan et al., 2015). However, the blood oxygen level dependent (BOLD) signal of fMRI may represent a mixture of different neurophysiological processes, and both the midbrain and basal forebrain contain a variety of different neurons (see Iglesias et al., 2013 for discussion). It is thus necessary to verify to what degree our previous findings truly reflect dopaminergic and cholinergic responses. Furthermore, a direct comparison between low-level PEs and high-level PEs in order to test for differential activations within the nuclei is not possible within the current analysis framework, as these regressors live on different scales; standardising (e.g. z-scoring) these regressors would change their interpretation and result in additional complex effects (Lebreton et al., 2019). Therefore, this study attempts to address the question of an involvement of dopamine in low-level PEs and acetylcholine in high-level PEs by using pharmacological manipulations of dopaminergic and cholinergic receptors in healthy volunteers.

Here, we present the results from two pharmacological fMRI study in healthy volunteers (N = 81 participants in each study; after exclusion, N = 75 (study 1) and N = 69 (study 2)). These studies employed selective dopaminergic and cholinergic antagonists (study 1: amisulpride and biperiden) and dopaminergic and cholinergic potentiating drugs (study 2: levodopa and galantamine), using the same computational modeling framework as in our previous study (Iglesias et al., 2013). The behavioural and fMRI data from one of the three groups in study 1 (the placebo group) have previously been published as part of Iglesias et al. (2013). Here we report differential effects of amisulpride/biperiden vs. placebo and levodopa/galantamine vs. placebo on the behavioural and fMRI data, as well as analyses where we averaged across all three pharmacological conditions within each study.

Based on our previous findings (Iglesias et al., 2013), our general hypothesis was that the precision-weighted outcome PE (ε_2) specifically reflects dopaminergic processes in the midbrain and that the precision-weighted probability PE (ε_3) is specifically related to cholinergic processes in the basal forebrain.

This general hypothesis allows for two more specific and testable predictions. Before we describe these in detail, it is worth pointing out that testing dopaminergic and cholinergic mechanisms with systemically active antagonists is complicated by the existence of two opposing pharmacological effects: on the one hand, antagonists can block inhibitory autoreceptors (located on somata and axon terminals), leading to disinhibition (Cragg and Greenfield, 1997). On the other hand, antagonists inhibit postsynaptic receptors; these could be located on neurons in remote projection sites (where they are activated by synaptic or volume transmission; Zoli et al., 1999; Cragg et al., 2001) or on nearby interneurons (where they are activated by paracrine release of transmitters; Zoli et al., 1999). This dual mode of action can make interpretations of pharmacological studies with systemic application difficult. For example, for amisulpride, it is assumed that low and high doses have opposite net effects, with inhibition of autoreceptors dominating at low doses and inhibition of postsynaptic receptors prevailing at high doses (Schoemaker et al., 1997; Rosenzweig et al., 2002). Similarly, the systemic application of pharmacological substances like levodopa and galantamine, which increase the availability of the respective neurotransmitter, does not allow for straightforward conclusions about which of the mechanisms mentioned above might dominate. Finally, in the absence of plasma level measurements and in order to (at least partially) account for individual differences in pharmacokinetics, we included body weight as a covariate in our second-level fMRI analyses. This was motivated by the fact that body weight is one factor of individual variability in pharmacokinetics, for example, because it can influence a drug's volume of distribution (with larger body weight typically associated with larger volume of distribution) and, for a given dose, plasma concentration decreases with the volume of distribution.

With these caveats in mind, a first prediction concerns activity in the neuromodulatory nuclei themselves. Specifically, a corollary of our general hypothesis is that one would expect to see that the midbrain activation by ε_2 and the basal forebrain activation by ε_3 are altered specifically by dopaminergic and cholinergic substances, respectively. This corresponds to the following interaction effects:

(i) The effect of ε_2 on midbrain activity should be altered significantly more strongly by amisulpride compared to biperiden and placebo, and by levodopa, compared to galantamine and placebo.[1]
(ii) The effect of ε_3 on basal forebrain activity should be altered significantly more strongly under biperiden compared to amisulpride and placebo, and under galantamine compared to levodopa and placebo.

Notably, either of these effects could be exerted by ε_2 or ε_3 *in toto* (as compound quantities) or could result from one of the components (i.e., the PE or the precision-weight).

A second (and equivalent) prediction concerns remote target areas of dopaminergic and cholinergic projections. Given the widespread distribution of cholinergic and, to a lesser degree, dopaminergic projections to the rest of the brain, it is more difficult to specify ex ante in which regions one expects possible alterations of PE-related activity by dopaminergic and cholinergic drugs (see Discussion). We therefore tested this prediction in a spatially less informed manner using whole-brain analyses.

In brief, our analyses examining precision-weighted PEs *in toto* and their separate components, respectively, did not provide clear-cut evidence for an unambiguous one-to-one relation between quantities from

[1] One would like to add the hypothesis "significantly more in the midbrain than in the basal forebrain". Testing this type of region-by-condition interaction, however, is prohibited in fMRI as the scaling of BOLD signal can differ across regions due to differences in neurovascular coupling.

our hierarchical Bayesian model and distinct neuromodulatory systems, as we had hoped to find. There are several reasons – in addition to this relation being truly absent, of course – that could explain our results. We discuss these possibilities in detail, outlining future tests based on the existing data. More generally, we use the current example, to showcase the complexities and ambiguities inherent to pharmacological fMRI.

2. Methods

2.1. Subjects

Eighty-one healthy male volunteers (mean age ± standard deviation, SD; study 1: 22 ± 2.4 years; study 2: 22 ± 3.0) participated in each of the two placebo-controlled double-blind pharmacological studies with a between-subject design. Within each study volunteers were randomly assigned to one of three pharmacological conditions such that each pharmacological condition contained twenty-seven volunteers. To exclude variations of hormonal effects on the BOLD signal (Goldstein et al., 2005), we only recruited male participants. Volunteers were all right-handed, non-smokers, without any psychiatric or neurological disorders in their past medical history, and were not taking any medication at the time. Additionally, before including volunteers in the study, an electrocardiogram (ECG) was recorded and evaluated by a board-certified cardiologist (R.M.) to exclude the presence of potentially arrhythmogenic cardiac predispositions that could have posed risks for pharmacological treatment. Notably, these studies were acquired consecutively and separately from each other. While the inclusion and exclusion criteria were identical in both studies, participants were not explicitly matched between studies, and no analyses between studies were performed. Participants were not explicitly matched across drug conditions either. However, our narrow inclusion and exclusion criteria prevented differences in most relevant variables except age. Age was not significantly different between drug groups in either of the studies (study 1: $F_{(2, 72)} = 0.467$, $p = 0.629$, $BF_{10} = 0.164$; study 2: $F_{(2, 66)} = 0.194$, $p = 0.824$, $BF_{10} = 0.141$).

Ethics approval was obtained by the locally responsible authorities (Kantonale Ethikkommission, KEK 2011-0101/3). All participants gave written informed consent before participating in the study.

Prior to data analysis, each subject's behavioural data (see below) were examined for invalid responses. Two behavioural measures were examined for each subject: trial-wise reaction times (RT) and percent correct responses (%CR). %CR measures were adjusted to account for the probabilistic nature of the task, that is, they were expressed in relation to the maximum %CR that an agent with perfect knowledge of the probabilistic task structure could achieve (i.e. 74%). Invalid trials were defined by the lack of any response (missed responses) or by excessively long reaction times (late responses; >1500 ms after cue presentation, i.e. at start of target presentation). Participants with more than 15% invalid trials or less than 65% CR were excluded from further analyses. These criteria led to the exclusion of five participants in study 1 (two from the amisulpride group and three from the biperiden group) and six participants in study 2 (three from the levodopa group, two from the placebo group, and one from the galantamine group). Furthermore, we had to exclude one participant per study due to claustrophobia (biperiden and galantamine group, respectively) and from study 2 two participants due to large movement artefacts (more than 40 additional regressors censoring scans with ≥1mm (translation) or ≥1º (rotation) scan-to-scan head movement; both from the galantamine group), one due to nausea (levodopa group), one due to drop-outs in the midbrain region in the fMRI data (galantamine group), and one due to problems with model-fitting of the winning model (galantamine group). As a consequence, the final data analysis included 75 participants (22 ± 2.3 years) in study 1 (25 participants in the amisulpride condition, 23 in the biperiden, and 27 in the placebo condition) and 69 participants (22 ± 3.1 years) in study 2 (22 participants in the levodopa condition, 22 in the galantamine, and 25 in the placebo condition).

2.2. Drug administration

Drug administration was performed in a randomised and double-blind fashion.

In study 1 each participant received either a single oral dose of the cholinergic (muscarinic) antagonist biperiden, the dopaminergic antagonist amisulpride, or placebo (lactose). Based on previous studies, dosage was chosen as 4 mg biperiden (Guthrie et al., 2000) or 400 mg of amisulpride (Rosenzweig et al., 2002), respectively. Drug administration took place 90 minutes before starting the first task (see below), as for both biperiden and amisulpride, the peak plasma level is attained within approximately 1.5 h (Grimaldi et al., 1986; Hamon-Vilcot et al., 1998).

In study 2 subjects received either a single oral dose of 8 mg galantamine (acetylcholinesterase inhibitor), 200 mg levodopa (prodrug of dopamine) combined with 50 mg of the peripheral decarboxylase inhibitor benserazide, or placebo (lactose). Drug administration started 60 min before starting the first task, as for both substances the peak plasma level is attained within approximately 1–2 h (Farlow, 2003; Khor and Hsu, 2007; Noetzli and Eap, 2013).

2.3. Experimental design: associative learning task

In both studies, participants performed the same audio-visual associative learning task (stimulus-stimulus learning, SSL) as described previously (fMRI study 2 in Iglesias et al., 2013; Iglesias et al., 2019). In brief, participants had to learn the predictive strengths of auditory cues (AC) in order to predict, as quickly and accurately as possible, which of two possible visual target (VT) categories would follow (a face or a house picture, Fig. 1A). Importantly, the cue-outcome association strength changed over time (volatility), including strongly predictive cues (probabilities of 0.9 and 0.1), moderately predictive cues (0.7, 0.3) and non-predictive cues (0.5; Fig. 1B). Participants were not informed about the sequence of probabilities. They were instructed explicitly that learning one association was sufficient to infer the entire probabilistic structure of the task (see Supplementary Material in Iglesias et al., 2013).

The two possible ACs, lasting for 300 ms, included high tones (576 Hz) and low tones (352 Hz), were followed by the VT (presented for 300 ms) 1200 ms later. During this interval, the participants had to indicate by button press whether they predicted a face or house to appear, providing us with an explicit behavioural readout of prediction (Fig. 1A). The appearance of the VT gave participants explicit feedback about their predictions and allowed them to update their beliefs trial-by-trial. There were no trial-wise monetary rewards. Participants received a fixed payment for participating in the study, which was independent of their task performance.

To ensure that participants perceived both tones equally loudly, they performed a psychophysical matching task within the MR scanner (den Ouden et al., 2010), prior to the task. Stimuli were presented using Cogent2000 (www.vislab.ucl.ac.uk/Cogent/index.html).

2.4. Questionnaires

To control for potential changes in vigilance and arousal due to the drugs, two questionnaires were applied: the Epworth Sleepiness Scale (ESS; Johns, 1991) and the Karolinska Sleepiness Scale (KSS; Akerstedt and Gillberg, 1990). However, only the KSS scores were used as covariates in the fMRI group analyses.

In the KSS, the subjective level of sleepiness at different time points during the day is measured. Here we explicitly asked them to rate their alertness during the fMRI measurements. Subjects had to indicate on a 9-point scale, from extremely alert (1) to extremely sleepy (9), which level best reflects their psycho-physical state (Akerstedt and Gillberg, 1990).

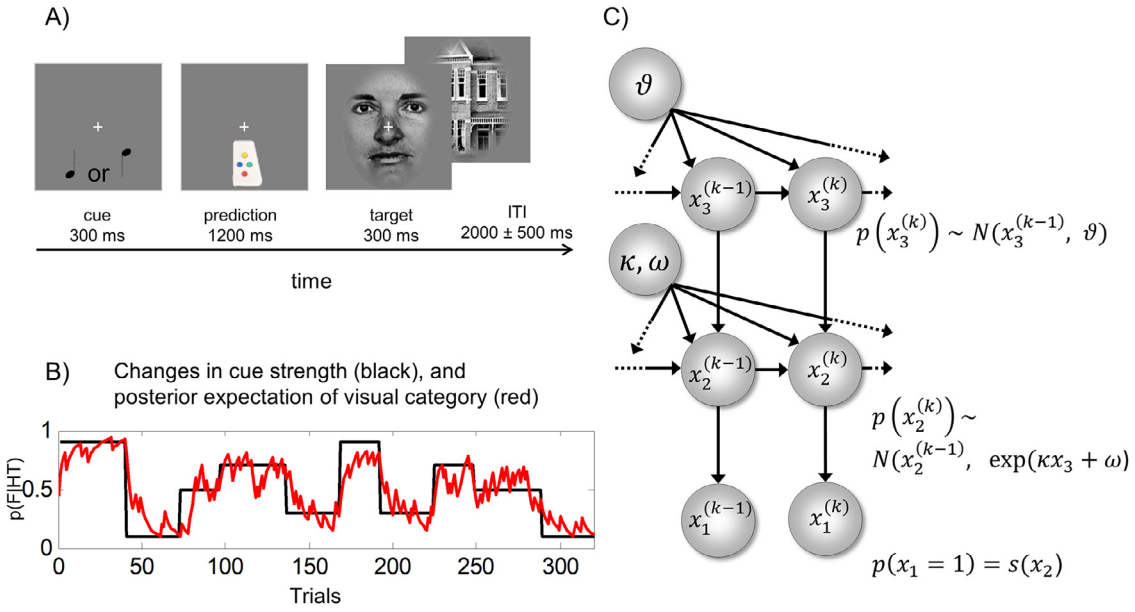

Fig. 1. Task and computational model

A) The sensory-sensory associative learning task (SSL). Subjects had to predict within 1200 ms which visual stimulus (face or house) followed an auditory cue (high or low tone). B) Black: the probabilistic trajectory visualizing the change in the association strength between the auditory cues and the visual targets, including high associations (probabilities of 0.9 and 0.1), moderate associations (0.7, 0.3) and no associations (0.5); red: trajectory example of a subject-specific posterior expectation of the visual outcome "Face" given the auditory high tone (HT). C) HGF: Hierarchical Gaussian Filter: x_1 represents the identity of the stimulus (stimulus category), x_2 the tendency towards one of the categories (the conditional probability of the target given the cue in logit space), and x_3 represents the (log) volatility of the environment. The figure has been adapted, with permission, from Iglesias et al. (2013).

2.5. Computational modeling of behavioural data

The behavioural data were analysed using the Hierarchical Gaussian Filter (HGF). This model describes hierarchical learning at multiple levels in terms of coupled Gaussian random walks (Mathys et al., 2011; Mathys et al., 2014). The update equations in this model are analytic and contain classical delta-rule or reinforcement learning as a special case, with precision-weighted PEs driving belief updating at different levels of the hierarchical model.

Here, we used an identical implementation of the HGF as in our previous study (Iglesias et al., 2013) and considered three alternative models: A first model, hgf_{3l}, corresponded to the standard three-level HGF as described by Mathys et al. (2011); Fig. 1C. For our learning task, the first level of this model represented the occurrence of the auditory and visual stimuli, the second level the conditional probability of the visual stimulus given the auditory cue, and the third level the change in this conditional probability (i.e., log-volatility). Free subject-specific learning parameters included ϑ (the speed of learning about the (log) volatility of the environment) and κ (which determined how much the estimated environmental volatility affected the learning rate at the second level). As explained in Mathys et al. (2014), for HGF applications where the belief trajectory at the third level does not inform the response model, not all of the perceptual parameters of the HGF are identifiable. Therefore, in order to ensure parameter identifiability we fixed the learning parameter ω (which is a constant component of the learning rate at the second level) to -4. The perceptual model was combined with a response model that linked trial-wise estimates of the conditional probability (of the visual stimulus given the auditory cue) to trial-wise behavioural responses (i.e., the subjects' predictions of visual stimulus category) by means of a sigmoid function with parameter ζ. This enabled us to invert the HGF in order to obtain subject-specific parameter estimates and belief trajectories (of PEs and precisions) for all levels of the model. However, it should be noted that for the behavioural analyses of the HGF parameters, we restricted ourselves to κ and ζ, which could be well recovered in simulations, whereas ϑ was not recoverable (see Figure S3, Supplementary Material).

The HGF software used for the analyses in this paper (hgfToolBox_v1.0) is available at www.translationalneuromodeling.org/tapas as open source code (GPLv3). All update equations are described in detail by Mathys et al. (2011, 2014).

Using random effects Bayesian model selection (BMS; Stephan et al., 2009; Penny et al., 2010), we compared this three-level HGF (hgf_{3l}) to two additional models: (i) a reduced model, hgf_{2l}, in which the third level (the log-volatility of the environment) was omitted; this represented the possibility that participants did not track and make use of volatility; and (ii), a non-hierarchical Rescorla-Wagner (RW) model with fixed learning rate. BMS operates on the log-evidence, which corresponds to the negative surprise of encountering the data given the model, and quantifies the trade-off between accuracy (fit) and model complexity. Please note that we could not use model "HGF_2" from Iglesias et al. (2013) because this referred to the prediction of trial-wise rewards – which did not exist in the present study.

Using the HGF we estimated subject-specific trajectories of different computational quantities that were used for subsequent fMRI analyses. In our first general linear model (GLM1) analysis of fMRI data, the following three quantities were used as parametric modulators, as in our previous analysis (Iglesias et al., 2013):

(i) ε_2 ($= \psi_2 \cdot \delta_1$), the precision-weighted PE about visual stimulus outcome[2] (which updates the estimate of visual stimulus probability in logit space, μ_2);

(ii) ε_3 ($\approx \psi_3 \cdot \delta_2$) the precision-weighted PE about visual stimulus probability[3] (which updates the estimate of environmental log volatility, μ_3);

[2] For the mathematical definition of precision weight ψ_2 and PE δ_1, see Eq. A.7 in Supplementary Material to Iglesias et al., 2013.

[3] For the mathematical definition of precision weight ψ_3 and PE δ_2, see Eq. A.10 in Supplementary Material to Iglesias et al., 2013.

(iii) ε_{ch}, the precision-weighted choice PE about visual stimulus outcome.

In a subsequent analysis (GLM2), we split the precision-weighted prediction errors into their components, resulting in the following parametric modulators:

(i) δ_1, the PE about visual stimulus outcome;
(ii) δ_2, the PE about visual stimulus probability;
(iii) ψ_2, precision weight at the second level; this corresponds to the learning rate by which visual stimulus probability estimates are updated;
(iv) ψ_3, precision weight at the third level; this is proportional to the learning rate by which (log) volatility estimates are updated;
(v) δ_{ch}, the choice PE about visual stimulus outcome.

Note that owing to the unambiguous nature of the outcomes, our sensory associative learning task involved informational uncertainty (or estimation uncertainty, i.e. the uncertainty about outcome probabilities, captured by ψ_2) and environmental uncertainty (i.e. changes in the probabilities with time, captured by ψ_3), but did not involve sensory uncertainty.

As the predictions in this task were of a categorical nature and the probabilities were coupled for both learning trajectories, we computed the absolute value of both, the precision-weighted prediction error (ε_2), and of the prediction error (δ_1) about the outcome (this is identical to computing separate trajectories for both stimulus categories; see Supplementary Material to Iglesias et al., 2013). Thus, the lower-level precision-weighted prediction error (ε_2) and the lower-level prediction error (δ_1) represent the difference between the actual visual outcome and its a priori probability. By contrast, the precision-weighted choice prediction error (ε_{ch}) and the lower-level prediction error (δ_{ch}) are signed prediction errors and represent the difference between the participant's choice being correct and the a priori probability of the correctness of this choice. Therefore, the choice prediction error is positive when the participant made a correct choice and negative when the participant was wrong (see Supplementary Material to Iglesias et al., 2013).

2.6. Classical inference

We performed univariate analyses of covariance (ANCOVA) to test whether there were significant differences in behaviour across the pharmacological conditions. For this we used the two HGF parameters, reaction time (RT), and percent correct responses (%CR) as dependent variables, weight, and KSS scores as covariates, and drug condition as independent variable. We report significant effects at a Bonferroni-corrected significance threshold of $0.05/4 = 0.0125$. Before running the ANCOVAs we verified that there were no differences across groups in the covariates. These statistical analyses were performed in IBM SPSS Statistics (Version 23.0).

At the suggestion of a reviewer we complemented our frequentist analyses with their Bayesian counterparts using the software JASP (Version 0.13.1; JASP Team, 2020) and report the corresponding Bayes factor expressed as BF_{10}, which is computed as the ratio between the probability of the data given the alternative hypothesis H_1 and the probability of the data given the null hypothesis H_0. As stated in Wagenmakers et al. (2018b), BF_{10} "... grades the degree of evidence that the data provided for H_1 versus H_0 ". According to their classification, a BF_{10} ranging from 3-10 reflects "moderate" evidence, a BF_{10} 1030 "strong" evidence, a BF_{10} 30-100 "very strong" evidence, and a BF_{10} >100 "extreme" evidence in favour of the alternative hypothesis (Wagenmakers et al., 2018a). For all Bayesian analyses, Cauchy prior distributions were used, as is default in JASP (Wagenmakers et al., 2018a). As a caveat, the current Bayesian ANOVA implementation does not account for potential violations of sphericity and normality, therefore, these results should be interpreted with caution (van den Bergh et al., 2020).

2.7. fMRI data acquisition and statistical analysis

In both studies structural and functional MRI data were acquired on a 3 Tesla Philips Achieva whole body MR Scanner (Philips Medical Systems) equipped with an eight-channel Philips SENSE head-coil. The structural image was acquired using a T_1-weighted sequence (inversion recovery MPRAGE sequence; resolution = 1.1 × 1.1 × 0.6 mm; inversion time (TI) = 875 ms; repetition time (TR) = 2.8 s). A $T_2{}^*$-weighted echo-planar imaging sequence covering the whole brain was used for functional data acquisition and lasted for ~ 23 min, or more specifically for 550 volumes with a TR of 2500 ms, a slice thickness of 3 mm; in-plane resolution of 2 × 2 mm; interslice gap of 0.6 mm; ascending continuous in-plane acquisition; TE = 36 ms; flip angle = 90°; field of view = 192 × 192 × 118 mm; SENSE factor = 2; EPI factor = 51 (as in Iglesias et al., 2013). A second order pencil-beam volume shim (provided by Philips) was applied to account for field inhomogeneities. The fMRI sequence we used was optimised for signal quality in brainstem and basal forebrain, resulting in signal dropouts in the orbitofrontal cortex (see Fig. S6). Therefore, no conclusions can be drawn about the representation of our computational quantities in this region.

In order to enable physiological noise correction of breathing and heart beat related signal variance, participants wore a breathing belt, and an electrocardiogram was obtained during fMRI data acquisition.

We analysed all fMRI data – including the placebo group data previously published in Iglesias et al. (2013) – using Statistical Parametric Mapping (SPM), version 12 (r7487). Preprocessing steps included motion correction of the functional images (realignment), co-registration to the structural image, warping of the functional and structural images to MNI space using the "New Segment" toolbox in SPM12, resampling to 1.5 × 1.5 × 1.5 mm resolution, and smoothing of the functional images with a 6 mm full-width at half maximum Gaussian kernel. Signal-to-noise ratio optimization for relevant regions such as the brain stem, was performed by correcting for physiological noise using RETROICOR (Glover et al., 2000) based on the PhysIO toolbox (expansion order of the regressors: 3rd, 4th, 1st order for cardiac, respiratory and interaction between respiratory and cardiac cycle, respectively (Harvey et al., 2008)) and by entering into the first-level GLMs regressors obtained from principal component analysis (PCA) of white matter and cerebrospinal fluid (CSF; Behzadi et al., 2007) using the PhysIO toolbox (version 2019b, v7.2.1) (Kasper et al., 2017; www.translationalneuromodeling.org/tapas).

We specified two different voxel-wise general linear models (GLMs) for each participant. In both of these first-level GLMs we specified regressors representing the two visual trial types (face, house), each of which was modulated by several computational quantities that were estimated from the individual behaviour. Specifically, in GLM1 we used the subject-specific trajectories of precision-weighted PEs ε_2, ε_3, ε_{ch} as computational (parametric) modulators. In GLM2 we split our computational quantities into precision and prediction error components, resulting in the following parametric modulators: δ_1, δ_2, ψ_2, ψ_3, δ_{ch}. In both GLMs, the regressors were not orthogonalised to each other and were time-locked to the outcome phase. Additionally, we modeled missed and late responses, respectively, by separate regressors. All regressors were convolved with a canonical hemodynamic response function and its temporal derivative.

In addition to these regressors of interest, our first-level GLMs also included regressors representing potential confounds. This included the realignment parameters, their first derivative, a regressor censoring scans with ≥1mm or ≥1º scan-to-scan head movement, physiological confound variables related to cardiac activity and breathing (provided by the PhysIO toolbox), and the PCA regressors for white matter and CSF.

Contrasts of interests at the first level included the average effect of each computational quantity (parametric modulator) specified above. These contrasts were entered into study-specific separate second (group) level ANOVAs (full factorial design) that compared the three different

drug groups, together with the two covariates (KSS score, and body weight). To test our hypotheses, we compared equivalent drug types across neuromodulators (i.e. amisulpride/biperiden/placebo and levodopa/galantamine/placebo). KSS accounted for individual variability in drug-induced vigilance. The covariate body weight was mean-centered and included an interaction with the factor drug. Body weight served as a proxy for the volume of distribution and thus as a (rough) approximation to individual differences in pharmacokinetics. In addition to testing for a main effect of drug, we tested whether drug effects on computational quantities showed a body-weight dependent effect.

In addition to whole-brain analyses, we performed region-of-interest (ROI) analyses based on a combined anatomical mask of putative dopaminergic and cholinergic nuclei, as in our previous study (Iglesias et al., 2013). The anatomical mask included (i) the dopaminergic midbrain (substantia nigra, SN, and ventral tegmental area, VTA; Bunzeck and Duzel, 2006), (ii) the cholinergic basal forebrain (Eickhoff et al., 2005; Zaborszky et al., 2008), and (iii) the putative cholinergic nuclei in the tegmentum of the brainstem, i.e., the pedunculopontine tegmental (PPT) and laterodorsal tegmental (LDT) nuclei. The latter were based on manual delineation using MRICron and anatomical landmarks (Naidich et al., 2009; Zrinzo et al., 2011).

Finally, we also had access to information about two single nucleotide polymorphisms (SNPs) in our volunteers: COMT (related to dopamine) and ChAT (related to acetylcholine; for more details, see Supplementary Material Section "Supplemental Results"). In order to explore interaction effects of the pharmacological intervention and computational quantities with genotype, we performed whole-brain and ROI group-level analyses as described previously, but adding COMT or ChAT as a covariate. However, as our sample size may not be sufficient for robust analyses of the influence by genotype, we report these results in the Supplementary Material only.

Our analyses focused on our anatomical regions of interest (ROIs), testing each computational quantity for group differences (e.g., differences in ε_2-related activity between biperiden and placebo). For the pharmacological effects in our ROIs, we use Bayesian statistics to assess the evidence for the null hypothesis relative to the alternative hypothesis. Since it is methodologically challenging to deal with spatial dependencies across voxels in current implementations of Bayesian tests when correcting for multiple comparisons, the Bayesian procedure we used differs from the statistical analysis performed with SPM. Specifically, for the Bayesian approach, we summarised the data across all voxels within a given ROI (in terms of the first eigenvariate) whereas for the SPM analyses we were performing voxel-wise analyses. More specifically, in the Bayesian approach we extracted the first eigenvariate (or principal component) separately for each region from our a priori anatomical mask, i.e., SN/VTA, basal forebrain, and PPT/LDT. This extraction was performed for each region separately, without applying any threshold, and removing all effects related to body weight and sleepiness. For each computational quantity and each of the three anatomical regions, the extracted first eigenvariates were entered into separate Bayesian ANOVAs, with the respective first eigenvariate as dependent variable, and group as independent variable. The model containing the factor group (H_1) was then compared to a null model (H_0). Post-hoc tests – i.e. pairwise comparisons with Bayesian t-tests using a Cauchy prior (0, $r = 1/\mathrm{sqrt}(2)$) – were only computed if the ANOVA displayed at least moderate evidence for the alternative hypothesis (i.e. if $BF_{10} > 3$). In JASP, multiple testing is accounted for by adjusting the prior odds. Multiplying the prior odds with the estimated BF results in the posterior odds (i.e. the relative plausibility of the model after observing the data (van Doorn et al., 2020).

Additionally, a number of regions throughout the brain showed significant drug effects on activity related to the different computational quantities. As these findings did not directly relate to our hypotheses, we report these results in the Supplementary Material (Tables S32 and S33). Regardless whether analyses were conducted for ROIs or across the whole brain, we always corrected stringently for multiple comparisons; in the former case, the search volume corresponded to the total volume of all ROIs combined. All findings reported in this paper survived family-wise error correction for multiple comparisons ($p < 0.05$), either at the peak-level or at the cluster-level with a cluster-defining threshold (CDT) of $p < 0.001$. This CDT affords valid cluster-level inference in SPM (see Eklund et al., 2016; Flandin and Friston, 2016).

3. Results

3.1. Behavioural data: classical analysis

Here, we report behavioural data from the $N = 75$ participants in study 1 and $N = 69$ in study 2, whose data were included in the fMRI analyses, respectively. First, within every study we tested for any significant differences in the sleepiness ratings (KSS) and body weight between the pharmacological groups. We did not find any significant group differences, neither in study 1 (KSS: $F_{(2,72)} = 0.229$, $p = 0.796$, $BF_{10} = 0.137$, i.e. the data is $1/0.137 = 7.3$ times more likely under H_0 than under H_1; body weight: $F_{(2,72)} = 1.354$, $p = 0.265$, $BF_{10} = 0.326$) nor in study 2 (KSS: $F_{(2,66)} = 1.012$, $p = 0.369$, $BF_{10} = 0.260$; body weight: $F_{(2,66)} = 0.674$, $p = 0.513$, $BF_{10} = 0.203$).

We subsequently performed one-way analyses (ANOVA) on reaction times (RT) and percent correct responses (%CR). Because normality and/or homoscedasticity were not always met, Welch's ANOVA was performed for all variables using drug as independent variable. Notably, using this test we cannot account for the effects of the covariates KSS and weight. We did not find any significant main effect of drug on these variables (study 1: RT: $F_{(2,\ 47.675)} = 0.621$, $p = 0.542$, $BF_{10} = 0.182$; %CR: $F_{(2,44.343)} = 1.193$, $p = 0.313$, $BF_{10} = 0.308$; study 2: RT: $F_{(2,\ 43.167)} = 0.567$, $p = 0.571$, $BF_{10} = 0.175$; %CR: $F_{(2,43.280)} = 1.544$, $p = 0.225$, $BF_{10} = 0.431$).

3.2. Behavioural data: computational modeling

Using Bayesian model selection (BMS; Stephan et al., 2009), we tested, following our previous study (Iglesias et al., 2013), which of several alternative generative models best explained our participants' behaviour. Specifically, we compared a three-level HGF model (hgf_{3l}), a reduced version of the HGF (hgf_{2l}), and the classical Rescorla-Wagner model (RW) of associative learning that has a fixed learning rate and is agnostic about environmental volatility. For BMS analyses we had to exclude participants due to numerical problems during inversion of the RW model (study 1: five participants excluded; study 2: four participants excluded) and inversion of the hgf_{3l} model (1 participant excluded from study 2 as listed in the "Subjects" session).

Independently of drug condition, random effects BMS yielded a posterior model probability (PP) of 87.0% and 79.9% in study 1 and study 2, respectively, and a protected exceedance probability of >0.99 in both studies in favor of model hgf_{3l}. This suggests that our participants not only learned the task-relevant conditional probabilities of visual stimuli, but were capable of tracking the volatility of the environment and updating their learning rate dynamically (Figure S4A and S5A, Table S3). (PP is the expected probability that the model in question generated the data for a randomly chosen subject. The exceedance probability (XP) of a model denotes the probability that this model has a greater posterior probability than any other model tested; and the protected exceedance probability (PXP) accounts for the possibility of models having identical frequencies; (Rigoux et al., 2014)). Furthermore, when each pharmacological condition was considered separately, hgf_{3l} was the most compelling of the models tested (study 1: placebo: PP = 87.9%, PXP > 99%; amisulpride: PP = 81.0%, PXP > 98%; biperiden: PP = 71.7%, PXP > 97.9%; Figure S4B-D, Table S3; study 2: placebo: PP = 65.0%, PXP > 94%; levodopa: PP = 85.9%, PXP > 99%; galantamine: PP = 72.2%, PXP > 93%; Figure S5B-D, Table S3).

Having identified an optimal model (amongst the models tested), we proceeded to testing whether within study there were significant differ-

ences in parameter estimates across drug conditions (see Table S4). (In the subsequent analyses, we excluded one subject for which we had encountered numerical fitting problems for hgf_{3l}). To this end, we performed Welch's one-way analyses of variance and a Bayesian ANOVA for the dependent variables κ (the learning parameter reflecting how much the estimated environmental volatility influences learning at the second level) and ζ (the parameter encoding decision noise in the observation model) with drug as independent variable. We did not find any significant main effect of drug on these model parameter estimates (study 1: κ: $F_{(2,44.937)} = 0.296$, $p = 0.745$, $BF_{10} = 0.157$; ζ: $F_{(2,45.737)} = 0.344$, $p = 0.711$, $BF_{10} = 0.144$; study 2: κ: $F_{(2,43.368)} = 1.237$, $p = 0.300$, $BF_{10} = 0.275$; ζ: $F_{(2,41.511)} = 2.375$, $p = 0.106$, $BF_{10} = 0.514$).

Finally, multiple regression was applied separately in both studies to test whether the model parameter estimates could explain task performance (percent correct responses (%CR)) and reaction times (RT) across all pharmacological conditions. Notably, if the identified model is reasonable, one would expect that it is associated with %CR but not RT; this is because the model was challenged to explain the binary nature of trial-by-trial decisions, but without reference to their speed. This test was conducted while controlling for potentially confounding factors in relation to pharmacology, i.e. KSS, and body weight. In a first step we only considered the confound variables and examined whether, on their own, they affected individual %CR. This was not the case in study 1: the combined influence of potential confounds only explained 6.5% of the variance in %CR (study 1; $F_{(2,72)} = 2.486$, $p = 0.09$; $BF_{10} = 0.627$). However, we found a significant influence in study 2 (R2 = 11.7%; $F_{(2,66)} = 4.388$, $p = 0.016$; $BF_{10} = 2.843$). Notably, this effect was only significant in the galantamine group (R2 = 30.6%; $F_{(2,19)} = 4.187$, $p = 0.031$; $BF_{10} = 2.434$).

We then added the two model parameter estimates (κ and ζ; Table S4) to the regression model; this explained additional 58.9% and 47.9% of the variance in %CR in study 1 and study 2, respectively (study 1: R2 change = 58.9; $F_{(2,70)} = 59.508$, $p < 0.001$; $BF_{10} > 150$; study 2: R2 change = 47.9; $F_{(2,64)} = 37.892$, $p < 0.001$; $BF_{10} > 150$). The main parameter driving this result was ζ (study 1: $\beta = 0.793$, $p < 0.001$; $BF_{Inclusion} > 150$; study 2: $\beta = 0.737$, $p < 0.001$, $BF_{Inclusion} > 150$; $BF_{Inclusion}$ represents the evidence in the data for including a predictor in the model (van den Bergh et al., 2020)). These results were not driven by any single pharmacological condition, but were found similarly when considering each drug in isolation (see Supplementary Material).

By contrast, as expected, adding the model parameter estimates to the regression model did not help explain RT (study 1: across conditions: R2 change = 0.02; $F_{(2,70)} = 0.822$, $p = 0.444$, $BF_{10} = 0.333$; study 2: across conditions: R2 change = 0.057; $F_{(2,64)} = 2.218$, $p = 0.117$, $BF_{10} = 0.844$).

Finally, it is worth noting that the behavioural results reported here (both in terms of model comparison and analyses of parameter estimates) are perfectly consistent with the results of the non-pharmacological fMRI study in Iglesias et al. (2013).

3.3. fMRI results

First, we tested for main effects of each computational variable (within every study pooled across drug conditions), both across the whole brain and within our anatomical mask (the combined ROIs of dopaminergic and cholinergic nuclei). This served to test whether, averaged across all pharmacological conditions, we would obtain comparable results to the non-pharmacological results as in Iglesias et al. (2013). For this, we used the same statistical criteria as in Iglesias et al. (2013), i.e., family-wise error correction for multiple comparisons ($p < 0.05$), at the peak-level.

Second, we tested for differential drug effects on the computational quantities and interaction effects between body weight, drug, and computational quantities; this test was applied both across the whole brain and within anatomically defined ROIs. As detailed in the Methods section, we only report results that survive FWE correction for multiple comparisons. Unless mentioned otherwise, the pharmacological results survive $p < 0.05$ at the cluster-level with a cluster-defining threshold (CDT) of $p < 0.001$.

Third, we conducted an alternative test of differential drug effects on the computational quantities using Bayesian ANOVAs (see Methods). Here, we focused on the three anatomical regions SN/VTA, BF and PPT/LDT within our a priori anatomical mask and assessed the evidence for a model including the pharmacological group factor compared to a null model.

As explained in the Methods, we used two different GLMs. In GLM1 we used precision-weighted PEs ($\varepsilon_2, \varepsilon_3, \varepsilon_{ch}$) as compound computational quantities for parametric modulation. In GLM2, we split these quantities into precision and PE components, resulting in five parametric modulators ($\delta_1, \delta_2, \psi_2, \psi_3, \delta_{ch}$).

3.3.1. GLM1: average effect of precision-weighted PEs across drug conditions

We first examined in both studies separately the low-level precision-weighted PEs, the absolute precision-weighted outcome PE ε_2 and the precision-weighted choice PE ε_{ch}. In both studies, whole-brain analyses showed a significant activation of numerous regions by ε_2, including parietal, prefrontal, visual, insular areas, and cerebellum (see Figs. 2A and 3A and Table S8). Additionally, we observed a deactivation of opercular, insular, cingulate, auditory, hippocampal and prefrontal areas (see Table S9 for details). The choice PE (ε_{ch}) not only activated a wide range of prefrontal, cingulate, insular, temporal, and parietal regions, but also ventral striatum, basal forebrain, putamen, and hippocampus (Figs. 2B and 3B, for a complete list, see Table S10). Deactivations by ε_{ch} were found in supplementary motor cortex, middle cingulate cortex, superior parietal cortex, middle frontal gyrus, calcarine cortex and precuneus (Table S11).

Within our anatomical mask, we found a significant ε_2 activation in the midbrain (as already observed in the whole brain analysis; see Figs. 2D and 3D for the anatomical ROI analysis), but also in PPT/LDT (Table S12) and a significant ε_2 deactivation in the basal forebrain (Table S13). Similarly, the choice prediction error ε_{ch} activated the basal forebrain (Figs. 2E and 3E, Table S14), as in the whole brain analysis, and deactivated in both studies putatively the cholinergic nuclei (PPT/LDT; Table S15) and additionally in study 1 the midbrain.

Subsequently, we moved to the next higher level of the hierarchy in our model and examined the precision-weighted probability PE, ε_3. In whole-brain analyses, we found ε_3 activations in the hippocampus, ACC, MCC opercular and insular regions (Figs. 2C and 3C Table S16). Deactivations were found in numerous regions, including occipital, insular, prefrontal, parietal, temporal areas as well as cerebellum (Table S17). Restricting the analyses to our anatomical mask, we found the expected ε_3 activation within the basal forebrain (Figs. 2F and 3F, Table S18) and a deactivation of the midbrain (Table S19).

3.3.2. GLM1: drug effects on precision-weighted PEs – ROI (anatomical mask)

In analyses restricted to our anatomical ROIs, we did not find significant differences between drug conditions for any of the computational quantities ($\varepsilon_2, \varepsilon_3, \varepsilon_{ch}$) that survived correction for multiple comparisons.

Using Bayesian ANOVA we tested, for each computational quantity and in each ROI (i.e. SN/VTA, BF, PPT/LDT), the evidence for a model that included the factor pharmacological group vs. a null model. For almost all tests, the Bayes factors showed that the data were better explained by the null model, although the evidence was only moderate at best (see Table S5). By contrast, evidence for drug effects was only found in one case (ε_3 in PPT/LDT, weak evidence).

3.3.3. GLM2: average effects of PEs and precisions across drug conditions

The prediction error about the outcome, δ_1 produced a similar whole-brain activation pattern as ε_2 (Figs. 4A and 5A), including prominent bilateral activations of prefrontal, parietal, insular, and cingulate areas as

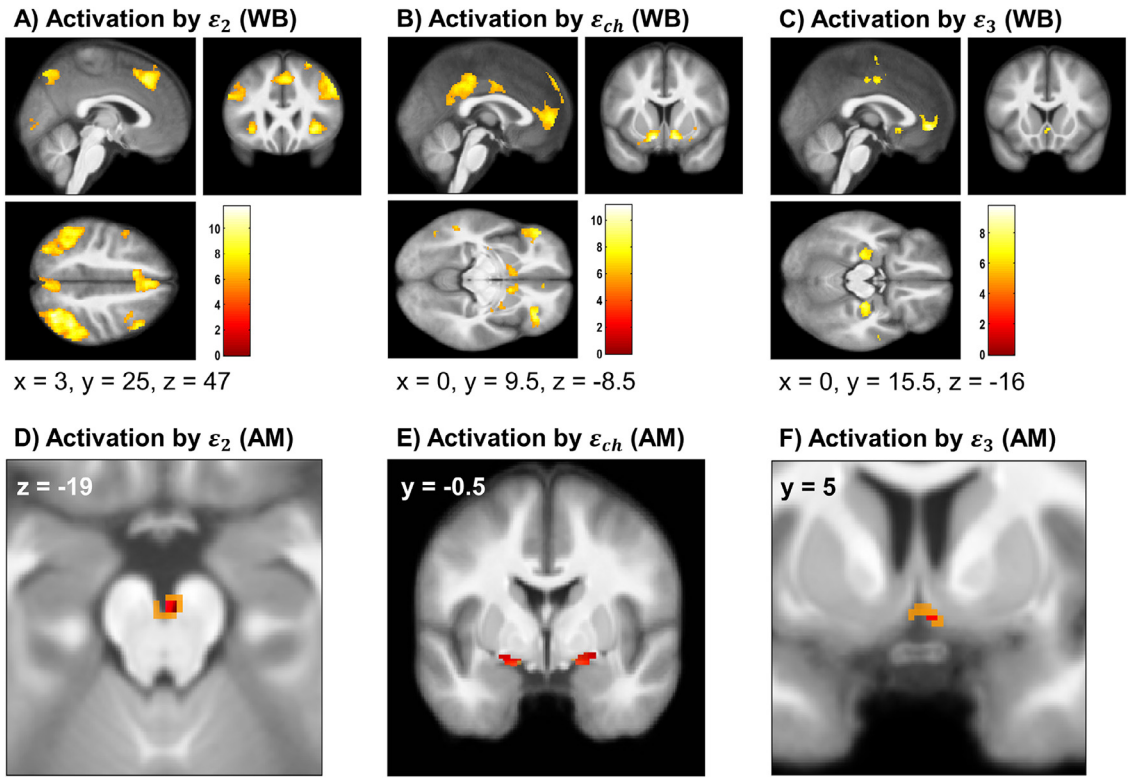

Fig. 2. Study 1 - Activations by the precision-weighted PEs
A) whole-brain activations by ε_2; B) whole-brain activations by ε_{ch}; C) whole-brain activations by ε_3; A-C) Activation maps are shown at a threshold of $p < 0.05$, FWE peak-level corrected for multiple comparisons across the whole brain. D) activations by ε_2; E) activations by ε_{ch}; F) activations by ε_3; D-F) Activation maps are shown at a threshold of $p < 0.05$, FWE peak-level corrected for multiple comparisons across the anatomical mask (red) overlayed on activation thresholded at $p < 0.05$, FWE cluster-level corrected for multiple comparisons with an initial CDT of $p < 0.001$ (orange). WB: whole-brain; AM: anatomical mask.

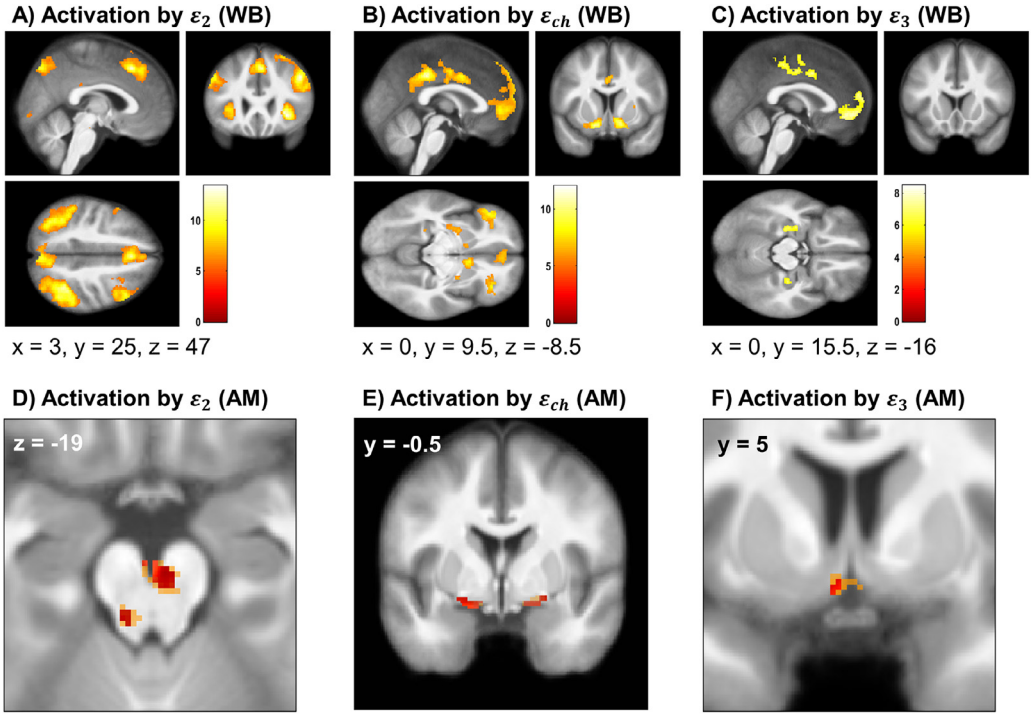

Fig. 3. Study 2 - Activations by the precision-weighted PEs
A) whole-brain activations by ε_2; B) whole-brain activations by ε_{ch}; C) whole-brain activations by ε_3; A-C) Activation maps are shown at a threshold of $p < 0.05$, FWE peak-level corrected for multiple comparisons across the whole brain. D) activations by ε_2; E) activations by ε_{ch}; F) activations by ε_3; D-F) Activation maps are shown at a threshold of $p < 0.05$, FWE peak-level corrected for multiple comparisons across the anatomical mask (red) overlayed on activation thresholded at $p < 0.05$, FWE cluster-level corrected for multiple comparisons with an initial CDT of $p < 0.001$ (orange). WB: whole-brain; AM: anatomical mask.

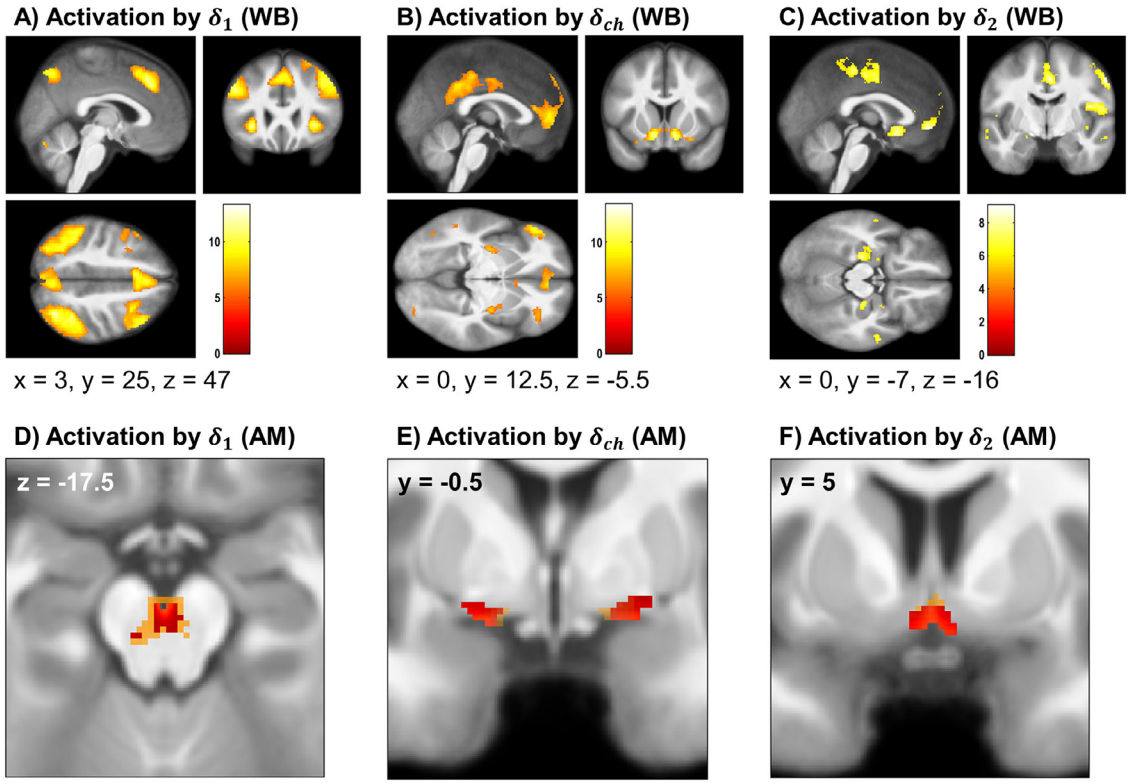

Fig. 4. Study 1 - Activations by the PEs
A) whole-brain activations by δ_1; B) whole-brain activations by δ_{ch}; C) whole-brain activations by δ_2; A-C) Activation maps are shown at a threshold of $p < 0.05$, FWE peak-level corrected for multiple comparisons across the whole brain. D) activations by δ_1; E) activations by δ_{ch}; F) activations by δ_2; D-F) Activation maps are shown at a threshold of $p < 0.05$, FWE peak-level corrected for multiple comparisons across the anatomical mask (red) overlayed on activation thresholded at $p < 0.05$, FWE cluster-level corrected for multiple comparisons with an initial CDT of $p < 0.001$ (orange). WB: whole-brain; AM: anatomical mask.

well as basal ganglia, thalamus, and (in study 2) midbrain (for detailed results, see Table S20). Deactivations were found in the basal forebrain, hippocampus, insula, as well as in various other cortical areas (Table S21).

In our anatomical mask we found a significant δ_1 activation within the midbrain and PPT/LDT (Figs. 4D and 5D). Deactivations were found in the septum and basal forebrain (spreading to parahippocampal gyrus but still within the probabilistically defined boundaries of the basal forebrain; Tables S22 and S23).

Concerning the choice prediction error, δ_{ch}, we found a similar activation pattern as compared to its precision-weighted counterpart, ε_{ch}, described above. This included activations in striatum, basal forebrain, vmPFC, mid and posterior cingulate cortex (for details and other activations, see Figs. 4B and 5B, and Table S24; for deactivations, see Table S25). In the anatomical ROI analyses, we found a δ_{ch} activation in bilateral basal forebrain (Figs. 4E and 5E, Table S26) and a deactivation in the putatively cholinergic nuclei and SN (Table S27).

Whole-brain analyses of the high-level prediction error (about probability), δ_2, activated the hippocampus and anterior cingulate gyrus as previously observed for its precision-weighted counterpart ε_3, but also the septum and middle cingulate gyrus (Figs. 4C and 5C; Table S28). Interestingly, the septal δ_2 activation was considerably stronger than for ε_3, suggesting that septal activity was more strongly driven by the PE than by precision. The δ_2 deactivations were similar to those for ε_3 (Table S29). In the anatomical ROI analyses, we found the expected activation of septum (Figs. 4F and 5F; Table S30), and deactivations in PPT/LDT and midbrain (Table S31).

Finally, we explored activity related to the precision weights. Notably, these precision weights have slightly different forms across the two levels of our model. At the lower (second) level, the precision weight ψ_2 corresponds to variance or uncertainty (about stimulus outcome); see Mathys et al. (2014). In whole-brain analyses, this quantity led to activations of angular and frontal gyri, parietal cortex, with additional activations in basal ganglia, anterior insula (only study 1) and cerebellum (Figs. 6A and 7A, Table S32). A deactivation was found in the right thalamus and precentral gyrus (Table S33). No results were found for ψ_2 in the anatomical ROI analyses.

Concerning the higher (third) level, the precision weight ψ_3 corresponds to a ratio of second- and third-level uncertainties; see Mathys et al. (2014) for details. For whole-brain analyses of ψ_3, we found significant activations of fusiform and lingual gyri, parietal, temporal, frontal areas, anterior insula and brainstem regions (Figs. 6B and 7B; Table S34; no overlapping deactivations across both studies were found; Table S35). Within our anatomical mask, we found an activation in the midbrain, and cholinergic nuclei PPT/LDT (Figs. 6D and 7D; Table S36).

3.3.4. GLM2: drug effects on PEs and precisions – ROI (anatomical mask)

For the low-level PE, we found that, compared to placebo, galantamine enhanced the positive relationship between body weight and δ_1-related activity in the midbrain (FWE peak-level and cluster-level corrected; x = 0; y = -27; z = -18; *t* score: 4.46; cluster size: 23 voxels; Fig. 8A). Furthermore, biperiden as opposed to placebo increased the δ_1-related activity in the right PPT/LDT (FWE peak-level corrected; x = 6; y = -36; z = -16; *t* score: 4.19; Fig. 9A). The same region (x = 6; y = -36; z = -18) showed a near-significant activation by δ_1 under amisulpride as compared to placebo (FWE peak-level corrected; *t* score: 3.99; p = 0.051).

For the high-level PE, we found that biperiden decreased δ_2-related activity in the right PPT/LDT (FWE peak-level corrected; x = 6; y = -36; z = -18; *t* score: 4.29; Fig. 9B). Additionally, we found a decreased δ_2-related activation in the right PPT/LDT under amisulpride as compared

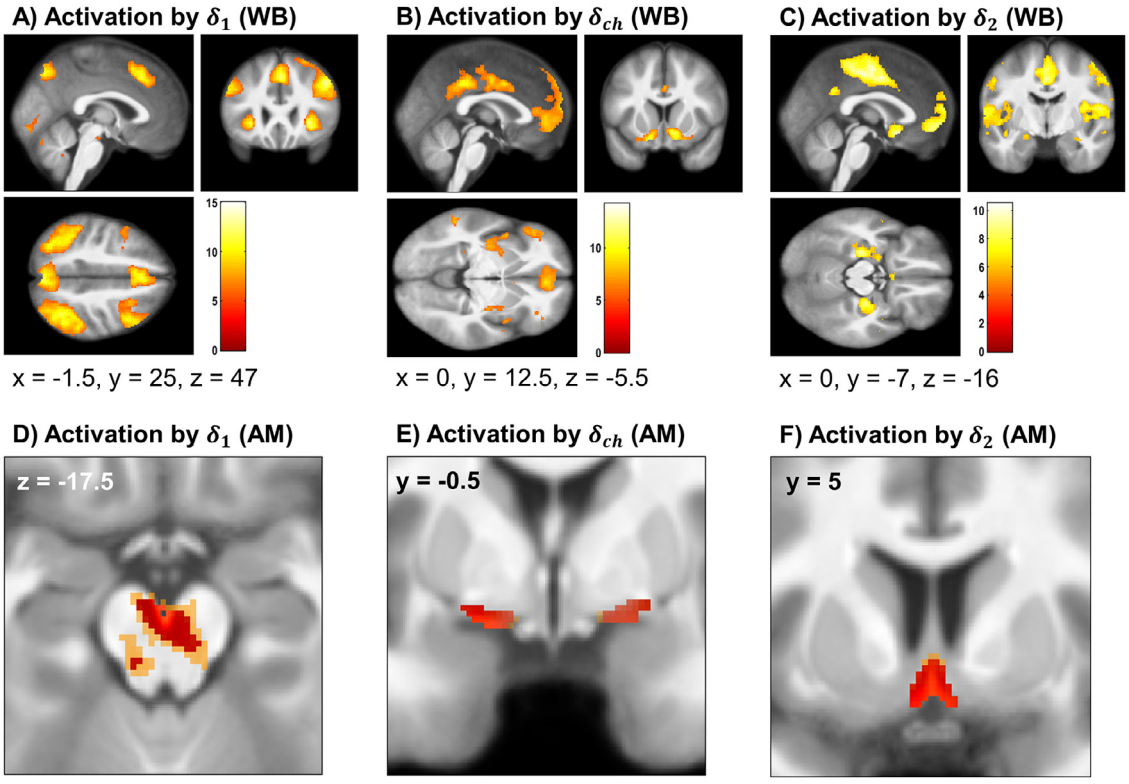

Fig. 5. Study 2 - Activations by the PEs
A) whole-brain activations by δ_1; B) whole-brain activations by δ_{ch}; C) whole-brain activations by δ_2; A-C) Activation maps are shown at a threshold of $p < 0.05$, FWE peak-level corrected for multiple comparisons across the whole brain. D) activations by δ_1; E) activations by δ_{ch}; F) activations by δ_2; D-F) Activation maps are shown at a threshold of $p < 0.05$, FWE peak-level corrected for multiple comparisons across the anatomical mask (red) overlayed on activation thresholded at $p < 0.05$, FWE cluster-level corrected for multiple comparisons with an initial CDT of $p < 0.001$ (orange). WB: whole-brain; AM: anatomical mask.

Table 1
Summary of all significant pharmacological effects on brain activity associated with our computational quantities in a priori anatomical regions of interest. Note that no effect was found for levodopa.

Computational quantity/anatomical region	δ_1 SN/VTA	ψ_3 SN/VTA		
galantamine	↑ vs. placebo interaction with body weight			
amisulpride		↑ vs. placebo		
Computational quantity/anatomical region	δ_1 PPT/LDT	δ_2 PPT/LDT	δ_2 PPT/LDT	δ_2 PPT/LDT
biperiden	↑ vs. placebo	↓ vs. placebo		
amisulpride			↓ vs. placebo	↑ vs. biperiden interaction with body weight

to placebo (FWE peak-level corrected; x = 6; y = -36; z = -18; *t* score: 5.30; Fig. 9C) and a modulation of drug effects on δ_2-related activity by body weight in right PPT/LDT (FWE peak-level corrected; x = 6; y = -34; z = -15; *t* score: 3.99): under amisulpride we found a positive relation between δ_2-related activity and body weight whereas this relation was inverted (negative) under biperiden (Fig. 9D). More precisely, δ_2-related activity in the PPT/LDT increased with lower body weight (and thus presumably higher plasma levels of biperiden) and with higher body weight (and hence putatively lower levels of amisulpride).

Finally, amisulpride compared to placebo increased the ψ_3-related activity in the midbrain (FWE peak-level and cluster-level corrected; x = 11; y = -25; z = -21; *t* score: 4.26; cluster size: 33 voxels; Fig. 8B).

There were no significant drug effects for δ_{ch}, ψ_2 in either study nor for any of the computational quantities in study 2, except for the one effect mentioned above (of galantamine on the relation between δ_1-related activity in the midbrain and body weight). All significant pharmacological effects across the anatomical mask have been summarized in Table 1.

In study 1, a Bayesian ANOVA found moderate evidence for a drug effect on δ_1-related activity in PPT/LDT ($BF_{10} = 9.105$). In line with the SPM results, Bayesian post-hoc tests revealed moderate evidence for a difference between placebo and biperiden (posterior odds = 4.924) and between placebo and amisulpride (posterior odds = 3.505; see Table S7). For the other regions (SN/VTA and basal forebrain), there was weak to moderate evidence in favour of the null model, i.e. absence of drug effects (see Table S6).

Finally, for all other computational quantities (except δ_2, were we found a weak effect in PPT/LDT) using Bayesian ANOVA the evidence showed that the data (extracted from the three anatomical regions, respectively) was best predicted by the null model (see Table S6).

4. Discussion

The notion that the different neuromodulatory transmitters – such as dopamine, acetylcholine, serotonin or noradrenaline – might serve to

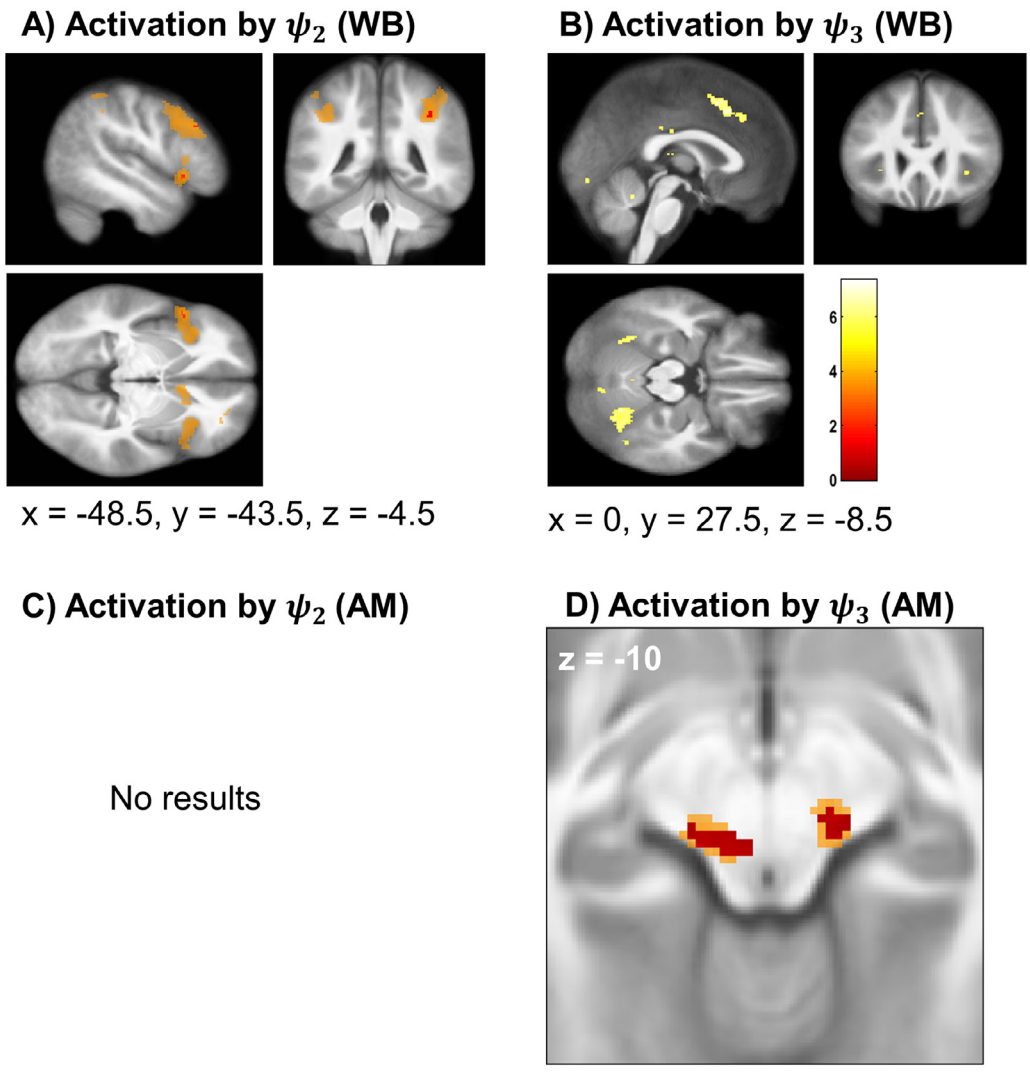

Fig. 6. Study 1 - Activations by the precision-weights
A) whole-brain activations by ψ_2; Activation maps are shown at a threshold of $p < 0.05$, FWE peak-level corrected for multiple comparisons across the whole brain (red) overlayed on activation thresholded at $p < 0.05$, FWE peak-level corrected for multiple comparisons with an initial CDT of $p < 0.001$ (orange).
B) whole-brain activations by ψ_3; Activation maps are shown at a threshold of $p < 0.05$, FWE peak-level corrected for multiple comparisons across the whole brain.
C) activations by ψ_2; D) activations by ψ_3; C-D) Activation maps are shown at a threshold of $p < 0.05$, FWE peak-level corrected for multiple comparisons across the anatomical mask (red) overlayed on activation thresholded at p < 0.05, FWE cluster-level corrected for multiple comparisons with an initial CDT of $p < 0.001$ (orange). WB: whole-brain; AM: anatomical mask.

signal distinct computational quantities has a long history (for reviews, see Doya, 2008; Dayan, 2012; Iglesias et al., 2017). A seminal finding was that phasic dopamine release appears to reflect reward PEs that may provide a teaching signal during instrumental learning (Schultz et al., 1997; Montague et al., 2004). Human fMRI studies have found representations of PEs in putative dopaminoceptive regions, such as the midbrain (D'Ardenne et al., 2008; Klein-Flugge et al., 2011; Diederen et al., 2016; Howard and Kahnt, 2018) or ventral striatum (Pessiglione et al., 2006; Glascher et al., 2010; Daw et al., 2011; Daniel and Pollmann, 2012; Hackel et al., 2015; Diederen et al., 2016; Guggenmos et al., 2016). Additionally, recent meta-analyses differentiating between absolute PEs (i.e. "surprise PE"; deviation between prediction and outcome) and signed PEs found that the former was represented in the putative dopaminergic midbrain, whereas the latter were represented in the ventral striatum (Garrison et al., 2013; Fouragnan et al., 2018). In our study, the low-level absolute PEs (δ_1 and precision-weighted ε_2, respectively) resemble the previously mentioned surprise PE and activated similar regions, such as the midbrain. Similarly, the choice PEs (δ_{ch} and precision-weighted ε_{ch}, respectively) showed a similar activation pattern as the signed PE. It must be kept in mind, however, that differences in interpretation exists between our Bayesian PEs and PEs from RL models. Whilst in RL the goal is to maximize reward, in our Bayesian framework the goal is to minimize (an approximation to) surprise by belief updating at multiple levels (Mathys et al., 2014), where the uncertainty of beliefs affects the way PEs impact on learning.

The signed choice PE computed in this study is different from the signed reward PE (RPE) used in RL: while RPEs encode whether an outcome was better (positive RPE) or worse than predicted (negative RPE; Schultz et al., 1997; Fouragnan et al., 2018), in our case the signed choice PE represents the difference between the participant's choice being correct and the a priori probability of this choice being correct (see Iglesias et al., 2013). Finally, our low-level absolute PE corresponds to Bayesian surprise, i.e. the difference between the outcome and its a priori probability.

Although RPEs and outcome PEs have been linked to dopamine, questions of specificity and context-dependency have arisen, even for

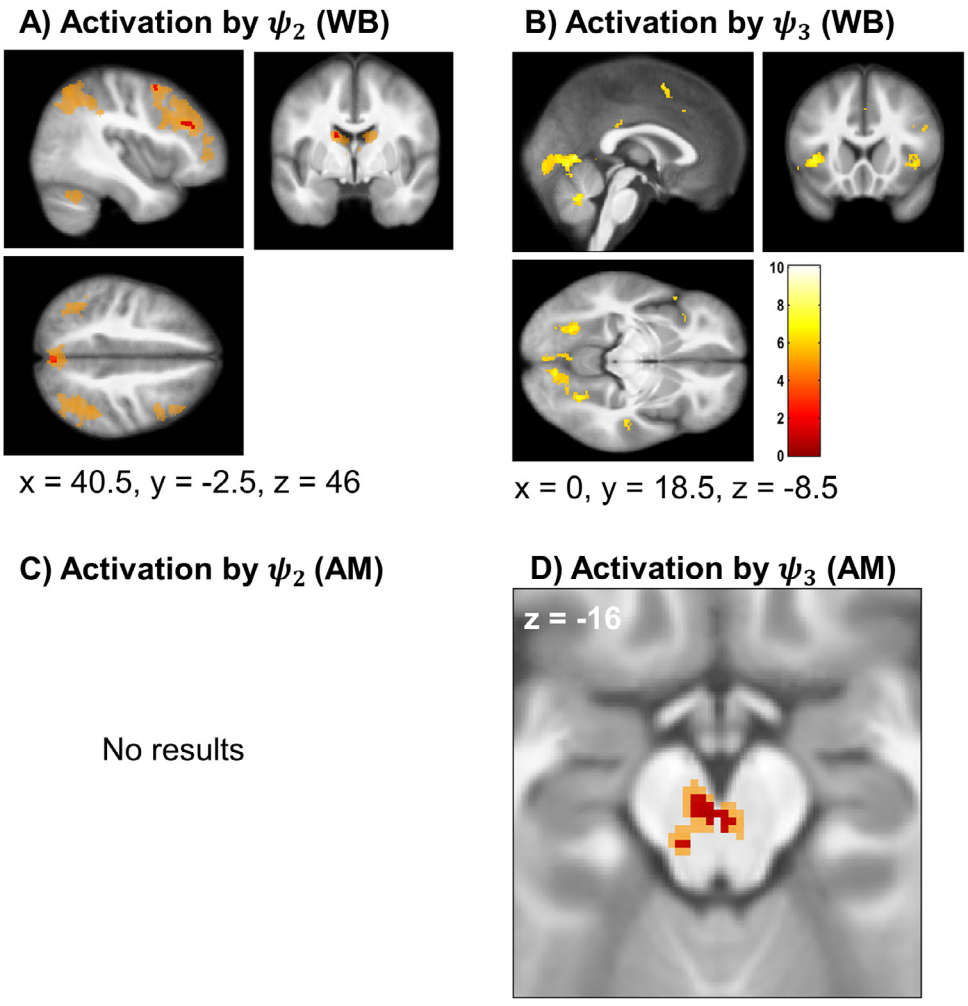

Fig. 7. Study 2 - Activations by the precision-weights
A) whole-brain activations by ψ_2; Activation maps are shown at a threshold of $p < 0.05$, FWE peak-level corrected for multiple comparisons across the whole brain (red) overlayed on activation thresholded at $p < 0.05$, FWE peak-level corrected for multiple comparisons with an initial CDT of $p < 0.001$ (orange).
B) whole-brain activations by ψ_3; Activation maps are shown at a threshold of $p < 0.05$, FWE peak-level corrected for multiple comparisons across the whole brain. C) activations by ψ_2; D) activations by ψ_3; C-D) Activation maps are shown at a threshold of $p < 0.05$, FWE peak-level corrected for multiple comparisons across the anatomical mask (red) overlayed on activation thresholded at $p < 0.05$, FWE cluster-level corrected for multiple comparisons with an initial CDT of $p < 0.001$ (orange). WB: whole-brain; AM: anatomical mask.

this most well-established link between neurotransmitters and computations. For example, recent work in humans using invasive voltammetry measurements of subsecond striatal DA release (Kishida et al., 2016) failed to find a simple link between reward PEs and DA release. Instead, this study suggested that striatal DA release reflects the integration of reward PEs with counterfactual prediction errors. More generally, dopamine was also found to support the formation of associations between neutral stimuli, without any reinforcement (Young et al., 1998). Furthermore, following human fMRI findings that suggested the signalling of sensory PEs by midbrain neurons (Iglesias et al. 2013), this has been corroborated by subsequent studies (Takahashi et al., 2017; Stalnaker et al., 2019), leading to the notion that dopamine transients might encode generalized PEs that are not necessarily tied to rewards (Gardner et al., 2018).

Beyond PEs, there are numerous studies indicating that dopamine might also signal uncertainty (or its inverse, precision) in a variety of contexts (Fiorillo et al., 2003; de Lafuente and Romo, 2011; Friston et al., 2012; Hart et al., 2015; Schwartenbeck et al., 2015). Altogether, these potentially diverse roles of dopamine could be interpreted as the possible reflection of a multiplexing principle (Nakahara, 2014; Gardner et al., 2018), where different computational quantities are broadcast in different frequency bands; this may be linked to differences in effects of phasic vs. tonic dopamine release (Grace, 1991). An alternative cause of diversity in dopamine function is the marked heterogeneity of dopamine neurons with regard to development, physiological properties and anatomical projection patterns (for review, see Roeper, 2013).

PEs and uncertainty/precision are fundamental components of many theories of learning and perceptual inference, and their signalling has also been linked to acetylcholine (Yu and Dayan, 2005; Okada et al., 2011; Moran et al., 2013; Vossel et al., 2014; Marshall et al., 2016; Naude et al., 2016), noradrenaline (Yu and Dayan, 2005; Payzan-LeNestour et al., 2013), and serotonin (Cohen et al., 2015). These attempts to understand the physiological implementations of computations have received considerable attention, not least because of their clinical implications: If a tight link between neuromodulators and specific computational quantities existed, this might enable the development of computational assays that inferred pathological alterations of neuromodulatory transmitters from combined behavioural and neuroimaging analyses (Stephan et al., 2015; Iglesias et al., 2017).

In a previous fMRI study using a sensory learning paradigm under volatility, we found (and replicated in two separate samples) that two hierarchically related PEs were reflected by activity in two neuromodulatory systems: low-level precision-weighted PEs about sensory outcomes activated the putative dopaminergic midbrain, whereas high-level precision-weighted PEs about the probability of the outcome activated the cholinergic basal forebrain (Iglesias et al., 2013), specifically the septum (Ch1-2 complex; Zaborszky et al., 2008). These results were intriguing since they suggested the feasibility of assaying two clinically relevant neuromodulatory systems with a single paradigm. However, as highlighted in this previous study, it was not possible to conclude with certainty that these fMRI results truly reflected DA and ACh signals. This is because the midbrain and basal forebrain are not exclusively composed of dopaminergic and cholinergic neurons, respectively, but

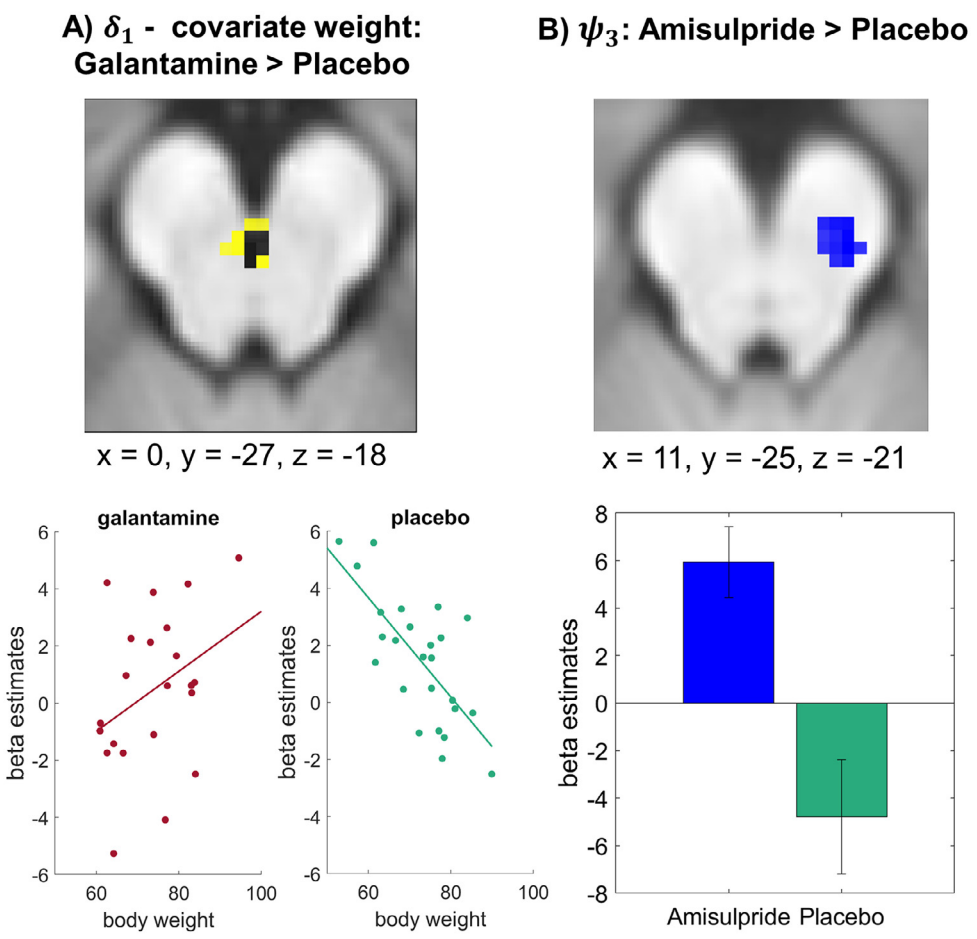

Fig. 8. Significant pharmacological results in the midbrain
A) Galantamine as compared to placebo increased the body-weight dependent δ_1 activity in the midbrain; the activation map is shown at a threshold of $p < 0.05$, FWE peak-level corrected for multiple comparisons across the anatomical mask (blue) overlayed on activation thresholded at $p < 0.05$, FWE cluster-level corrected for multiple comparisons with an initial CDT of $p < 0.001$ (yellow). B) Amisulpride as compared to placebo increased the ψ_3-related activity in the midbrain; the activation map is shown at a threshold of $p < 0.05$, FWE cluster-level corrected for multiple comparisons across the whole brain, with an initial CDT of $p < 0.001$. The data were extracted from the significant peak voxel at the group level, removing the effects of group and sleepiness (A) or removing the effects of the covariates body weight and sleepiness (B), respectively.

contain numerous types of neurons, e.g. GABAergic and glutamatergic neurons (for reviews, Zaborszky and Duque, 2003; Duzel et al., 2009). Additionally, dopaminergic midbrain neurons receive cholinergic afferents (Bolam et al., 1991; Oakman et al., 1995; Yeomans et al., 2001; Kobayashi and Okada, 2007), and cholinergic basal forebrain neurons receive dopaminergic inputs (Gaykema and Zaborszky, 1996). These two factors complicate the interpretation of midbrain/basal forebrain activations considerably, as both dopaminergic and cholinergic mechanisms could explain activation of either region. To add even more complexity, cholinergic mechanisms can not only alter the firing pattern of DA neurons in midbrain (e.g., Yeomans et al., 2001; Kobayashi and Okada, 2007), but can also trigger striatal DA release via presynaptic receptors on mesostriatal projections and independently so from DA neuron activity (Threlfell et al., 2012).

The present study represents an initial attempt to scrutinize the interpretability of our previous fMRI findings by investigating how pharmacological perturbations of DA and ACh would alter the representation of precision-weighted PEs in dopaminergic and cholinergic nuclei. In humans, this can only be tested by systemic administration of drugs, in combination with human neuroimaging. (Unfortunately, as discussed below, this approach has many possible confounds and limitations.) Here, for two separate studies, we used a between-subject design where participants in study 1 either received 400 mg of the D2/D3-receptor antagonist amisulpride, 4 mg of the muscarinic (M1) receptor antagonist biperiden, or placebo, and in study 2 either 200 mg of the prodrug levodopa combined with 50 mg of benserazide, 8 mg of the acetylcholinesterase inhibitor galantamine, or placebo. The ideal result we hoped to find was that low- and high-level precision-weighted PE activity in the midbrain and basal forebrain would be selectively affected by pharmacological manipulations of DA and ACh, respectively.

This hypothesis was not supported by our data. In brief, we did not find clear-cut evidence for a dichotomy between low-level precision-weighted PEs and DA on the one hand, and high-level precision-weighted PEs and ACh on the other hand. This hypothesised dichotomy did not emerge either when splitting the precision-weighted PEs in their PE and precision components. We did, however, find effects of interest across the anatomical ROIs that deserve discussion.

First, we found a body-weight dependent pharmacological effect on δ_1-related activity in the SN/VTA: compared to placebo, galantamine enhanced the positive relation between body weight and low-level PE (δ_1)-related activity in this region (Fig. 8A). More specifically, δ_1-related midbrain activity decreased with higher body weight in the placebo condition but increased under galantamine. While the cholinergic effect on the midbrain is not directly in line with our previous hypothesis and the current literature linking sensory PEs to midbrain DA signalling, the effects of galantamine might have occurred via cholinergic receptors on dopaminergic midbrain neurons. For example, cholinergic projections from PPT and LDT affect DA neuron activity via both nicotinic and muscarinic receptors (Zhou et al., 2003). Galantamine is an acetylcholinesterase inhibitor enhancing ACh levels and also acts as allosteric modulator of presynaptic nicotinic ACh receptors, increasing receptor sensitivity (Noetzli and Eap, 2013). Most studies examining the activation of nicotinic and muscarinic receptors on DA midbrain neurons have found excitatory effects (e.g. Dani and Bertrand, 2007; Schilstrom et al., 2007; Blaha et al., 1996; for review, Zhou et al., 2003). Unless these effects follow a nonlinear dose-response relationship, they should decrease with higher body weight (and thus presumably lower plasma levels of galantamine), whereas we found the opposite. Activation of muscarinic receptors on dopamine neurons in the SN/VTA can also exert inhibitory effects on midbrain dopamine neurons but this may be re-

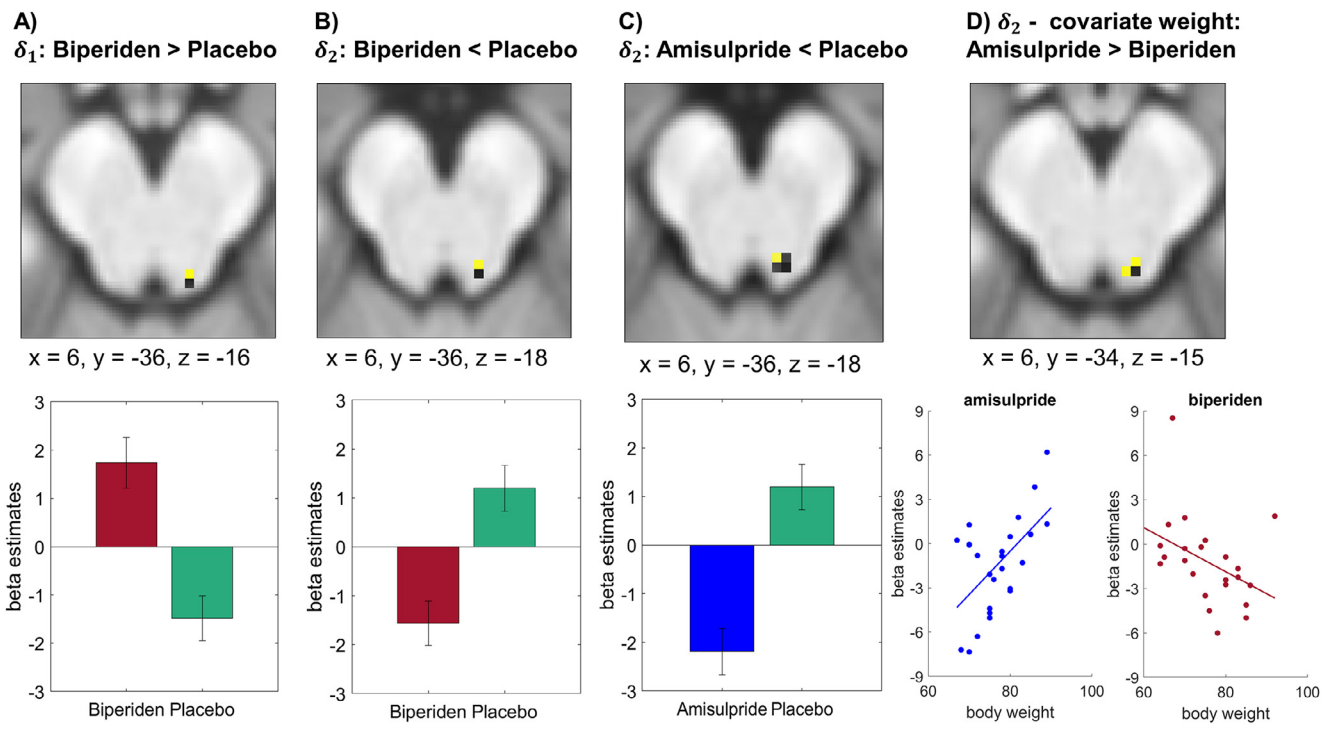

Fig. 9. Significant pharmacological results in putatively the cholinergic nuclei
A) Biperiden as compared to placebo increased the δ_1-related activity in PPT/LDT; B) biperiden as compared to placebo reduced the δ_2-related activity in PPT/LDT; C) amisulpride as compared to placebo reduced the δ_2-related activity in PPT/LDT; D) amisulpride as compared to biperiden increased the body-weight dependent δ_2-related activity in PPT/LDT. The fMRI results overlayed on the structural image are shown at a threshold of $p < 0.05$, FWE peak-level corrected for multiple comparisons across the whole brain (blue) and uncorrected at the cluster-level, with an initial CDT of $p < 0.001$ (yellow). The data were extracted from the significant peak voxel at the group level, removing the effects of the covariates body weight and sleepiness (A, B, C) or removing the effects of group and sleepiness (D), respectively.

stricted to phasic cholinergic transmission (Fiorillo and Williams, 2000; but see Miller and Blaha, 2005). In brief, it is not immediately clear how the observed increase in δ_1-related midbrain activity with higher body weight (and thus presumably lower galantamine levels) can be reconciled with the known interactions between the dopaminergic midbrain and cholinergic PPT/LDT.

A second finding was that biperiden affected low-level PEs (δ_1) and the high-level PE (δ_2) in a brainstem region corresponding to putatively the cholinergic PPT/LDT (Fig. 9A and B, regions overlap). These effects were independent of body weight, i.e. reflecting mean pharmacological effects on activity in PPT/LDT related to both prediction errors. This is partly compatible with our previous study (Iglesias et al., 2013) – where we had found an activation of the precision-weighted high-level PE in a cholinergic region, the basal forebrain – and results from recent behavioural studies that used the HGF and cholinergic manipulations (Vossel et al., 2014; Marshall et al., 2016). The biology behind possible dopaminergic and cholinergic effects on PPT/LDT activity, however, is complex and deserves a brief discussion to illustrate the numerous ways in which drugs can affect these nuclei and their interactions with the dopaminergic midbrain. PPT/LDT not only contain cholinergic, but also glutamatergic, GABAergic and dopaminergic neurons (Pahapill and Lozano, 2000; Kobayashi and Okada, 2007; Okada et al., 2011), receive cholinergic, glutamatergic and GABAergic afferents (Ye et al., 2010), and project widely to other (sub)cortical regions, including the dopaminergic midbrain (Lodge and Grace, 2006; von Bohlen und Halbach & Dermietzel, 2006; Mena-Segovia et al., 2008; Okada et al., 2011). Projections from the SN to PPT include both inhibitory and excitatory connections (Granata and Kitai, 1991; Okada et al., 2011), and SN neurons are endowed with muscarinic receptors (Vilaró et al., 1990; Levey et al., 1991; Zubieta and Frey, 1993). Furthermore, the PPT receives input from the ventral pallidum which, in turn, receives GABAergic projections from the dopaminergically innervated ventral striatum (Lee et al., 2000). This circuitry offers ample targets for DA and ACh in affecting PPT/LDT activity.

A third finding was that amisulpride significantly increased activation of the right midbrain by ψ_3, the precision-weight on the third level of our model (Fig. 8B); this particular precision-weight corresponds to the degree of the agent's uncertainty about the log-volatility $x_3^{(k)}$ (i.e. the precision that modulates the influence of the high-level PE on log-volatility estimates). In the placebo condition SN responses were negatively related to the participant's precision-weight at the third level, and this negative relation disappeared under amisulpride and turned into a positive relation. The precision of beliefs about action selection has been related to dopaminergic processes (de Lafuente and Romo, 2011; Schwartenbeck et al., 2015; Parr and Friston, 2017), while expected uncertainty (i.e. the difference between the degree (conditional probability) of cue validity and certainty) has been linked to cholinergic signalling (Yu and Dayan, 2005; Iglesias et al., 2013; Parr and Friston, 2017) and unexpected uncertainty (uncertainty about state transitions) to noradrenergic signalling (Yu and Dayan, 2005; Payzan-LeNestour et al., 2013; Parr and Friston, 2017). Here we find a dopaminergic modulation of ψ_3-related activity in a dopaminergic region, suggesting a dopaminergic role in signalling higher level precision estimates (as further shown by the average effect of ψ_3).

Our second hypothesis concerning pharmacological effects on representations of the computational quantities across the whole-brain was more exploratory. Nevertheless, given the prominence of certain neuroanatomically characterised projections, for the lower-level computational quantities (ε_2, δ_1, and ψ_2) effects would have been expected in major dopaminergic projection regions such as the basal ganglia, hippocampus, amygdala, cingulate and frontal cortex (Wise, 2004; Bentivoglio and Morelli, 2005; Schultz, 2012) and for the higher-level

computational quantities (ε_3, δ_2, and ψ_3) in cholinergic projection regions such as the cortex, hippocampus, amygdala, thalamus and hypothalamus (Mesulam et al., 1983; Newman et al., 2012).

Our whole-brain analyses did not result in a clear picture of how (sub)cortical activity related to the different computational quantities was modulated by the different drugs. We therefore only shortly summarise some of the whole-brain drug effects found compared to placebo (see Tables 37 and 38 in the Supplementary Material for all whole-brain pharmacological effects).

Some of the dopaminergic effects were in line with expectations, for example, under amisulpride we found a deactivation by the lower-level precision-weighted PE, ε_2, in the putamen and the lower-level precision-weight, ψ_2, activity in the caudate (a body-weight dependent effect). Furthermore, we found that levodopa increased δ_1-related activity in the inferior parietal cortex. However, we also found unexpected dopaminergic effects. For example, in the caudate, we found an unexpected dopaminergic effect on the higher-level PE, with amisulpride decreasing δ_2-related activity, and we found increased δ_1 activity in the caudate under amisulpride (i.e. as opposed to the deactivation we expected under 400mg of amisulpride).

For the cholinergic drugs, we found, consistent with our expectations, that biperiden reduced activation by the higher-level PE, δ_2, in the cuneus. By contrast, galantamine unexpectedly reduced δ_2-dependent activity in the anterior insula, middle cingulate cortex, precuneus, supramarginal, angular, and middle frontal gyrus (a body-weight dependent effect). Furthermore, we found unexpected cholinergic effects on cortical activity related to the lower-level precision-weighted PE ε_2 (e.g. a body-weight dependent increase of activity in the superior frontal gyrus and angular gyrus under galantamine) and the lower-level PE δ_1 (e.g. reduced activity in the cuneus under biperiden) (for details see Tables 37 and 38).

Returning to our main hypothesis, what are the possible reasons that we failed to find the expected dichotomy between low-level precision-weighted PEs and DA on the one hand, and high-level precision-weighted PEs and ACh on the other hand? A first obvious reason is that our hypotheses were simply false, and the expected effects do not exist (or are too subtle to be detected under the power that our experiment affords). Having said this, a number of previous results did support a relation between the computational quantities we tested and DA/ACh. For example, with regard to ACh, its link to the high-level precision-weighted PE ε_3 is not only motivated theoretically by the concept of "expected uncertainty" (Yu and Dayan 2005; see Supplementary Material in Iglesias et al 2013), but supported by findings from two behavioural studies (Vossel et al., 2014; Marshall et al., 2016). Notably, both of these studies used a learning paradigm with volatility and employed the same type of computational model (i.e., three-level HGF) as our study. Vossel et al. (2014) boosted ACh levels using the AChE inhibitor galantamine and found the expected increase in high-level precision-weighted PEs (Vossel et al., 2014). Marshall et al. (2016) used the muscarinic receptor antagonist biperiden and reported the opposite effect on high-level precision-weighted PEs; however, these effects were not specific, and biperiden was found to influence more computational variables.

A second potential reason is that we may have failed to achieve sufficiently high plasma levels of our drugs. Given that this was a basic science study with healthy volunteers and that the drugs used can have non-trivial side effects, we wished to minimise any risks for the participants. We therefore administered the drugs only once and chose a minimal dose (400 mg amisulpride, 4 mg biperiden; 8 mg galantamine, 200 mg levodopa combined with 50 mg of benserazide). This dose may have turned out to be too low; a possibility that is suggested by the lack of any behavioural drug effects in our study (for comparison, Marshall et al. 2016 found marked effects of biperiden during a similar learning paradigm using 6 mg biperiden, i.e., a dose that was 50% higher than ours). Furthermore, since we did not obtain individual drug plasma levels, we decided to use body weight as a proxy variable. This was done in order to account (at least approximately) for the volume of distribution, one of several factors that determine inter-individual variability in pharmacokinetics (see below). Clearly, this is a crude approximation since the relation between body weight and volume of distribution is not necessarily linear for a given drug.

A third possible reason is that pharmacological fMRI suffers from several general methodological limitations and problems of interpretation in general. To begin with, for many neurophysiological and cognitive processes pronounced individual differences in drug effects have been observed (for a review on dopamine in this regard, see Cools and D'Esposito, 2011). This heterogeneity has multiple sources, including individual differences in effectively achieved drug concentrations (pharmacokinetics) and in drug efficacy *per se* (pharmacodynamics: the relation between concentration and effect of a drug; for review, see Roden and George, 2002). These differences can be substantial – for example, the pharmacokinetics of dopamine in healthy individuals differs by more than a factor of 10 (MacGregor et al., 2000) – and may explain why, under the same drug intervention, different individuals are pushed to either side of frequently observed convex dose-response relationships (e.g., "inverted U"; Cools and D'Esposito, 2011; Pearson-Fuhrhop et al., 2013).

In addition to this individual variability, human pharmacological fMRI experiments can be difficult to interpret. One issue is that the consequences of systemically administered drugs can fundamentally differ across the brain, not only depending on which receptor subtypes are present in a given region, but also whether presynaptic (autoreceptors) or postsynaptic receptors are primarily affected by the drug at the chosen dose (Schoemaker et al., 1997; Rosenzweig et al., 2002). For example, as presynaptic D2 receptors (autoreceptors) can be activated at lower dopamine levels than postsynaptic D2 receptors, low doses of a dopaminergic challenge could mainly act on autoreceptors, whereas at high doses postsynaptic receptors are more strongly, but not exclusively, affected (Beaulieu and Gainetdinov, 2011). Amisulpride seems to conform to this profile and exert mainly presynaptic effects on dopamine autoreceptors at low doses and therefore enhance dopamine neuron activity (Di Giovanni et al., 1998) and dopamine release (Lieberman, 2004), whereas at higher doses it additionally (and possibly more strongly) affects postsynaptic dopamine D2 and D3 receptors (Rosenzweig et al., 2002). Disambiguating these two opposing effects is difficult under systemic administration (cf. van der Schaaf et al., 2014). Finally, drug can exert vascular effects in addition to neuronal ones. For example, neuroanatomical and neurophysiological evidence exists that both dopaminergic and cholinergic (muscarinic) drugs affect vascular tone and thus hemodynamic signals such as cerebral blood flow (e.g., Vaucher and Hamel, 1995; Krimer et al., 1998; Choi et al., 2006; Lecrux et al., 2017).

Another potential limitation of our study is that the type of task employed here – a sensory prediction task that was deliberately speeded to avoid the possibility that subjects might be employing complex cognitive strategies not easily captured by the type of learning models considered here – necessitates an experimental design in which cues and outcomes are temporally close together. Additionally, a fixed time interval between cue and outcome is mandatory in order to avoid temporal prediction errors. In BOLD measurements, this can induce high correlations in the respective signals; an issue that can be aggravated when using temporal derivatives to account for variability in the onset of BOLD responses. In principle, it is thus possible that some or even all of our PE results could reflect trial-wise prediction effects. However, animal studies (with electrophysiological techniques that have much higher temporal resolution and avoid such correlations) only found that DA neuron activity reflected trial-wise sensory PEs, but failed to find any relation between DA neuron activity and trial-wise predictions about sensory features of the outcome (for summary, see discussion in Takahashi et al., 2017). While we cannot fully rule out that the situation may differ in humans, we therefore do not consider the design of our task a severe limitation for the interpretation of our results.

Finally, one of the strengths of our study – the computational analysis of expressed behaviour – also constitutes a potential limitation. As any computational model, the analysis relies on hypotheses about the cognitive strategy employed by participants. Although several alternatives are compared formally (Bayesian model selection), our modelling approach probably does not capture the full variability of cognitive strategies likely employed by our participants. Furthermore, although BMS identified the same model as most plausible in all pharmacological conditions, the differences between models varied, suggesting that cognitive strategies may have been modulated by the drug applied.

Given these many possible confounds and problems of interpretation, our present results may not decisively refute our initial hypothesis. In future studies and analyses, we hope to extend the present analyses in several ways in order to rule out vascular effects and control for individual differences in pharmacokinetics. For example, we have conducted EEG studies with a similar task and measuring individual plasma levels. This approach will not allow for investigating activity in brainstem nuclei, unfortunately. Furthermore, we are considering to move to within-subject cross-over designs as the presence vs. absence of drug in the same subject enables new types of analyses that can detect undirected drug effects, absorbing much of the inter-individual variability discussed above (for a compelling demonstration of this approach, see Piray et al., 2017). We hope that further studies of this sort will help clarify the nature of the hypothesised relation between low- and high-level PEs on the one hand and dopaminergic and cholinergic processes on the other hand.

Author contributions

Funding was provided by KES. SI and KES designed the study and wrote the manuscript. LK defined the fMRI sequences and performed fMRI quality checks. RM analysed and controlled all ECGs. SI collected the data and performed the analyses with the support of KES, CM (modeling) and LK (PhysIO). SH performed the code review. All authors contributed to editing the manuscript.

Data and code availability

Upon acceptance of this paper, the behavioural and smoothed fMRI data will be made publicly available on the ETH Research Collection (a freely accessible repository that conforms to the FAIR principles). The code used for the analysis will be made publicly available on the GIT repository of ETH Zurich (https://gitlab.ethz.ch/tnu/code/iglesiasetal_neuromodulation_sensory_learning_2020). All relevant third-party dependencies are clearly indicated and are freely available. Furthermore, the code has been cross-checked internally for reproducibility. The anatomical masks used are not openly available online.

Declaration of Competing Interest

The authors have declared no conflicts of interest for this article.

Acknowledgments

We acknowledge support by the Zurich Neuroscience Centre (SI, KES), by the René and Susanne Braginsky Foundation (KES), and the University of Zurich (KES). S.J.H. was also supported by the grant #2017-403 of the Strategic Focal Area “Personalized Health and Related Technologies (PHRT)” of the ETH Domain. We are very grateful to Jan Mauer for performing the SNP analyses and to Marc Tittgemeyer for procedural and logistic support. We thank Simon Eickhoff and Emrah Düzel for providing us with the anatomical masks for delineating the basal forebrain and VTA/SN, respectively. We also thank Karl Treiber, Katharina Woog, Etna Engeli, Franziska Dahinden and Anh Thu Pham for their support during data acquisition.

Supplementary materials

Supplementary material associated with this article can be found, in the online version, at doi:10.1016/j.neuroimage.2020.117590.

References

Akerstedt, T., Gillberg, M., 1990. Subjective and objective sleepiness in the active individual. Int. J. Neurosci. 52, 29–37. doi:10.3109/00207459008994241.
Beaulieu, J.M., Gainetdinov, R.R., 2011. The physiology, signaling, and pharmacology of dopamine receptors. Pharmacol. Rev. 63, 182–217. doi:10.1124/pr.110.002642.
Behrens, T.E., Woolrich, M.W., Walton, M.E., Rushworth, M.F., 2007. Learning the value of information in an uncertain world. Nat. Neurosci. 10, 1214–1221. doi:10.1038/nn1954.
Behzadi, Y., Restom, K., Liau, J., Liu, T.T., 2007. A component based noise correction method (CompCor) for BOLD and perfusion based fMRI. Neuroimage 37, 90–101. doi:10.1016/j.neuroimage.2007.04.042.
Bentivoglio, M., Morelli, M., 2005. Chapter I The organization and circuits of mesencephalic dopaminergic neurons and the distribution of dopamine receptors in the brain. In: Dunnett, M.B.A.B., S.B., Hökfelt, T. (Eds.), Handbook of Chemical Neuroanatomy. Elsevier, pp. 1–107.
Blaha, C.D., Allen, L.F., Das, S., Inglis, W.L., Latimer, M.P., Vincent, S.R., Winn, P., 1996. Modulation of dopamine efflux in the nucleus accumbens after cholinergic stimulation of the ventral tegmental area in intact, pedunculopontine tegmental nucleus-lesioned, and laterodorsal tegmental nucleus-lesioned rats. J. Neurosci. 16, 714–722. doi:10.1523/jneurosci.16-02-00714.1996.
Bolam, J.P., Francis, C.M., Henderson, Z., 1991. Cholinergic input to dopaminergic neurons in the substantia nigra: a double immunocytochemical study. Neuroscience 41, 483–494. doi:10.1016/0306-4522(91)90343-m.
Bunzeck, N., Duzel, E., 2006. Absolute coding of stimulus novelty in the human substantia nigra/VTA. Neuron 51, 369–379. doi:10.1016/j.neuron.2006.06.021.
Choi, J.K., Chen, Y.I., Hamel, E., Jenkins, B.G., 2006. Brain hemodynamic changes mediated by dopamine receptors: Role of the cerebral microvasculature in dopamine-mediated neurovascular coupling. Neuroimage 30, 700–712. doi:10.1016/j.neuroimage.2005.10.029.
Cohen, J.Y., Amoroso, M.W., Uchida, N., 2015. Serotonergic neurons signal reward and punishment on multiple timescales. Elife 4. doi:10.7554/eLife.06346.
Cools, R., D'Esposito, M., 2011. Inverted-U-shaped dopamine actions on human working memory and cognitive control. Biol. Psychiatry 69, e113–e125. doi:10.1016/j.biopsych.2011.03.028.
Cragg, S.J., Greenfield, S.A., 1997. Differential autoreceptor control of somatodendritic and axon terminal dopamine release in substantia nigra, ventral tegmental area, and striatum. J. Neurosci. 17, 5738–5746.
Cragg, S.J., Nicholson, C., Kume-Kick, J., Tao, L., Rice, M.E., 2001. Dopamine-mediated volume transmission in midbrain is regulated by distinct extracellular geometry and uptake. J. Neurophysiol. 85, 1761–1771.
D'Ardenne, K., McClure, S.M., Nystrom, L.E., Cohen, J.D., 2008. BOLD responses reflecting dopaminergic signals in the human ventral tegmental area. Science 319, 1264–1267. doi:10.1126/science.1150605.
Dani, J.A., Bertrand, D., 2007. Nicotinic acetylcholine receptors and nicotinic cholinergic mechanisms of the central nervous system. Annu. Rev. Pharmacol. Toxicol. 47, 699–729. doi:10.1146/annurev.pharmtox.47.120505.105214.
Daniel, R., Pollmann, S., 2012. Striatal activations signal prediction errors on confidence in the absence of external feedback. Neuroimage 59, 3457–3467. doi:10.1016/j.neuroimage.2011.11.058.
Daw, N.D., Gershman, S.J., Seymour, B., Dayan, P., Dolan, R.J., 2011. Model-based influences on humans' choices and striatal prediction errors. Neuron 69, 1204–1215. doi:10.1016/j.neuron.2011.02.027.
Dayan, P., 2012. Twenty-five lessons from computational neuromodulation. Neuron 76, 240–256. doi:10.1016/j.neuron.2012.09.027.
Dayan, P., Hinton, G.E., Neal, R.M., Zemel, R.S., 1995. The Helmholtz machine. Neural Comput. 7, 889–904. doi:10.1162/neco.1995.7.5.889.
de Lafuente, V., Romo, R., 2011. Dopamine neurons code subjective sensory experience and uncertainty of perceptual decisions. Proc. Natl. Acad. Sci. USA 108, 19767–19771. doi:10.1073/pnas.1117636108.
den Ouden, H.E., Daunizeau, J., Roiser, J., Friston, K.J., Stephan, K.E., 2010. Striatal prediction error modulates cortical coupling. J. Neurosci. 30, 3210–3219. doi:10.1523/JNEUROSCI.4458-09.2010.
Di Giovanni, G., Di Mascio, M., Di Matteo, V., Esposito, E., 1998. Effects of acute and repeated administration of amisulpride, a dopamine D2/D3 receptor antagonist, on the electrical activity of midbrain dopaminergic neurons. J. Pharmacol. Exp. Ther. 287, 51–57.
Diaconescu, A.O., Mathys, C., Weber, L.A.E., Kasper, L., Mauer, J., Stephan, K.E., 2017. Hierarchical prediction errors in midbrain and septum during social learning. Soc. Cognit. Affect. Neurosci. 12, 618–634. doi:10.1093/scan/nsw171.
Diederen, K.M., Spencer, T., Vestergaard, M.D., Fletcher, P.C., Schultz, W., 2016. Adaptive prediction error coding in the human midbrain and striatum facilitates behavioral adaptation and learning efficiency. Neuron 90, 1127–1138. doi:10.1016/j.neuron.2016.04.019.
Doya, K., 2008. Modulators of decision making. Nat. Neurosci. 11, 410–416. doi:10.1038/nn2077.
Duzel, E., Bunzeck, N., Guitart-Masip, M., Wittmann, B., Schott, B.H., Tobler, P.N., 2009. Functional imaging of the human dopaminergic midbrain. Trends Neurosci. 32, 321–328. doi:10.1016/j.tins.2009.02.005.

Eickhoff, S.B., Stephan, K.E., Mohlberg, H., Grefkes, C., Fink, G.R., Amunts, K., Zilles, K., 2005. A new SPM toolbox for combining probabilistic cytoarchitectonic maps and functional imaging data. Neuroimage 25, 1325–1335. doi:10.1016/j.neuroimage.2004.12.034.

Eklund, A., Nichols, T.E., Knutsson, H., 2016. Cluster failure: why fMRI inferences for spatial extent have inflated false-positive rates. Proc. Natl. Acad. Sci. USA 113, 7900–7905. doi:10.1073/pnas.1602413113.

Farlow, M.R., 2003. Clinical pharmacokinetics of galantamine. Clin. Pharmacokinet. 42, 1383–1392. doi:10.2165/00003088-200342150-00005.

Felleman, D.J., Van Essen, D.C., 1991. Distributed hierarchical processing in the primate cerebral cortex. Cereb. Cortex 1, 1–47. doi:10.1093/cercor/1.1.1.

Fiorillo, C.D., Tobler, P.N., Schultz, W., 2003. Discrete coding of reward probability and uncertainty by dopamine neurons. Science 299, 1898–1902. doi:10.1126/science.1077349.

Fiorillo, C.D., Williams, J.T., 2000. Cholinergic inhibition of ventral midbrain dopamine neurons. J. Neurosci. 20, 7855–7860. doi:10.1523/jneurosci.20-20-07855.2000.

Flandin, G. & Friston, K.J. 2016. Analysis of family-wise error rates in statistical parametric mapping using random field theory. arXiv preprint arXiv:1606.08199.

Fouragnan, E., Retzler, C., Philiastides, M.G., 2018. Separate neural representations of prediction error valence and surprise: evidence from an fMRI meta-analysis. Hum. Brain Map. 39, 2887–2906. doi:10.1002/hbm.24047.

Friston, K., 2005. A theory of cortical responses. Philos. Trans. R Soc. Lond. B Biol. Sci. 360, 815–836. doi:10.1098/rstb.2005.1622.

Friston, K.J., Shiner, T., FitzGerald, T., Galea, J.M., Adams, R., Brown, H., Dolan, R.J., Moran, R., Stephan, K.E., Bestmann, S., 2012. Dopamine, affordance and active inference. PLoS Comput. Biol. 8, e1002327. doi:10.1371/journal.pcbi.1002327.

Gardner, M.P.H., Schoenbaum, G., Gershman, S.J., 2018. Rethinking dopamine as generalized prediction error. Proc. Biol. Sci. 285, 20181645. doi:10.1098/rspb.2018.1645.

Garrison, J., Erdeniz, B., Done, J., 2013. Prediction error in reinforcement learning: a meta-analysis of neuroimaging studies. Neurosci. Biobehav. Rev. 37, 1297–1310. doi:10.1016/j.neubiorev.2013.03.023.

Gaykema, R.P., Zaborszky, L., 1996. Direct catecholaminergic-cholinergic interactions in the basal forebrain. II. Substantia nigra-ventral tegmental area projections to cholinergic neurons. J. Comp. Neurol. 374, 555–577 10.1002/(SICI)1096-9861(19961028)374:4<555::AID-CNE6>3.0.CO;2-0.

Glascher, J., Daw, N., Dayan, P., O'Doherty, J.P., 2010. States versus rewards: dissociable neural prediction error signals underlying model-based and model-free reinforcement learning. Neuron 66, 585–595. doi:10.1016/j.neuron.2010.04.016.

Glover, G.H., Li, T.Q., Ress, D., 2000. Image-based method for retrospective correction of physiological motion effects in fMRI: RETROICOR. Magn. Reson. Med. 44, 162–167 10.1002/1522-2594(200007)44:1<162::aid-mrm23>3.0.co;2-e.

Goldstein, J.M., Jerram, M., Poldrack, R., Ahern, T., Kennedy, D.N., Seidman, L.J., Makris, N., 2005. Hormonal cycle modulates arousal circuitry in women using functional magnetic resonance imaging. J. Neurosci. 25, 9309–9316. doi:10.1523/JNEUROSCI.2239-05.2005.

Grace, A.A., 1991. Phasic versus tonic dopamine release and the modulation of dopamine system responsivity: a hypothesis for the etiology of schizophrenia. Neuroscience 41, 1–24. doi:10.1016/0306-4522(91)90196-u.

Granata, A.R., Kitai, S.T., 1991. Inhibitory substantia nigra inputs to the pedunculopontine neurons. Exp. Brain Res. 86, 459–466. doi:10.1007/BF00230520.

Grimaldi, R., Perucca, E., Ruberto, G., Gelmi, C., Trimarchi, F., Hollmann, M., Crema, A., 1986. Pharmacokinetic and pharmacodynamic studies following the intravenous and oral administration of the antiparkinsonian drug biperiden to normal subjects. Eur. J. Clin. Pharmacol. 29, 735–737. doi:10.1007/BF00615970.

Guggenmos, M., Wilbertz, G., Hebart, M.N., Sterzer, P., 2016. Mesolimbic confidence signals guide perceptual learning in the absence of external feedback. Elife 5. doi:10.7554/eLife.13388.

Guthrie, S.K., Manzey, L., Scott, D., Giordani, B., Tandon, R., 2000. Comparison of central and peripheral pharmacologic effects of biperiden and trihexyphenidyl in human volunteers. J. Clin. Psychopharmacol. 20, 77–83. doi:10.1097/00004714-200002000-00013.

Hackel, L.M., Doll, B.B., Amodio, D.M., 2015. Instrumental learning of traits versus rewards: dissociable neural correlates and effects on choice. Nat. Neurosci. 18, 1233–1235. doi:10.1038/nn.4080.

Hamon-Vilcot, B., Chaufour, S., Deschamps, C., Canal, M., Zieleniuk, I., Ahtoy, P., Chretien, P., Rosenzweig, P., Nasr, A., Piette, F., 1998. Safety and pharmacokinetics of a single oral dose of amisulpride in healthy elderly volunteers. Eur. J. Clin. Pharmacol. 54, 405–409. doi:10.1007/s002280050483.

Hart, A.S., Clark, J.J., Phillips, P.E.M., 2015. Dynamic shaping of dopamine signals during probabilistic Pavlovian conditioning. Neurobiol. Learn. Mem. 117, 84–92. doi:10.1016/j.nlm.2014.07.010.

Harvey, A.K., Pattinson, K.T., Brooks, J.C., Mayhew, S.D., Jenkinson, M., Wise, R.G., 2008. Brainstem functional magnetic resonance imaging: disentangling signal from physiological noise. J. Magn. Reson. Imaging 28, 1337–1344. doi:10.1002/jmri.21623.

Hilgetag, C.C., O'Neill, M.A., Young, M.P., 2000. Hierarchical organization of macaque and cat cortical sensory systems explored with a novel network processor. Philos. Trans. R. Soc. Lond. B Biol. Sci. 355, 71–89. doi:10.1098/rstb.2000.0550.

Howard, J.D., Kahnt, T., 2018. Identity prediction errors in the human midbrain update reward-identity expectations in the orbitofrontal cortex. Nat. Commun. 9, 1611. doi:10.1038/s41467-018-04055-5.

Iglesias, S., Mathys, C., Brodersen, K.H., Kasper, L., Piccirelli, M., den Ouden, H.E., Stephan, K.E., 2013. Hierarchical prediction errors in midbrain and basal forebrain during sensory learning. Neuron 80, 519–530. doi:10.1016/j.neuron.2013.09.009.

Iglesias, S., Mathys, C., Brodersen, K.H., Kasper, L., Piccirelli, M., den Ouden, H.E.M., Stephan, K.E., 2019. Hierarchical prediction errors in midbrain and basal forebrain during sensory learning. Neuron 101, 1196–1201. doi:10.1016/j.neuron.2019.03.001.

Iglesias, S., Tomiello, S., Schneebeli, M., Stephan, K.E., 2017. Models of neuromodulation for computational psychiatry. Wiley Interdiscip. Rev. Cognit. Sci. 8. doi:10.1002/wcs.1420, n/a-n/a.

Johns, M.W., 1991. A new method for measuring daytime sleepiness: the Epworth sleepiness scale. Sleep 14, 540–545. doi:10.1093/sleep/14.6.540.

Kasper, L., Bollmann, S., Diaconescu, A.O., Hutton, C., Heinzle, J., Iglesias, S., Hauser, T.U., Sebold, M., Manjaly, Z.M., Pruessmann, K.P., Stephan, K.E., 2017. The PhysIO toolbox for modeling physiological noise in fMRI data. J. Neurosci. Methods 276, 56–72. doi:10.1016/j.jneumeth.2016.10.019.

Khor, S.P., Hsu, A., 2007. The pharmacokinetics and pharmacodynamics of levodopa in the treatment of Parkinson's disease. Curr. Clin. Pharmacol. 2, 234–243. doi:10.2174/157488407781668802.

Kishida, K.T., Saez, I., Lohrenz, T., Witcher, M.R., Laxton, A.W., Tatter, S.B., White, J.P., Ellis, T.L., Phillips, P.E., Montague, P.R., 2016. Subsecond dopamine fluctuations in human striatum encode superposed error signals about actual and counterfactual reward. Proc. Natl. Acad. Sci. USA 113, 200–205. doi:10.1073/pnas.1513619112.

Klein-Flugge, M.C., Hunt, L.T., Bach, D.R., Dolan, R.J., Behrens, T.E., 2011. Dissociable reward and timing signals in human midbrain and ventral striatum. Neuron 72, 654–664. doi:10.1016/j.neuron.2011.08.024.

Kobayashi, Y., Okada, K., 2007. Reward prediction error computation in the pedunculopontine tegmental nucleus neurons. Ann. N. Y. Acad. Sci. 1104, 310–323. doi:10.1196/annals.1390.003.

Krimer, L.S., Muly, E.C., Williams, G.V., Goldman-Rakic, P.S., 1998. Dopaminergic regulation of cerebral cortical microcirculation. Nat. Neurosci. 1, 286–289. doi:10.1038/1099.

Lebreton, M., Bavard, S., Daunizeau, J., Palminteri, S., 2019. Assessing inter-individual differences with task-related functional neuroimaging. Nat. Hum. Behav. 3, 897–905. doi:10.1038/s41562-019-0681-8.

Lecrux, C., Sandoe, C.H., Neupane, S., Kropf, P., Toussay, X., Tong, X.K., Lacalle-Aurioles, M., Shmuel, A., Hamel, E., 2017. Impact of altered cholinergic tones on the neurovascular coupling response to whisker stimulation. J. Neurosci. 37, 1518–1531. doi:10.1523/JNEUROSCI.1784-16.2016.

Lee, M.S., Rinne, J.O., Marsden, C.D., 2000. The pedunculopontine nucleus: its role in the genesis of movement disorders. Yonsei Med. J. 41, 167–184. doi:10.3349/ymj.2000.41.2.167.

Levey, A.I., Kitt, C.A., Simonds, W.F., Price, D.L., Brann, M.R., 1991. Identification and localization of muscarinic acetylcholine receptor proteins in brain with subtype-specific antibodies. J. Neurosci. 11, 3218–3226.

Lieberman, J.A., 2004. Dopamine partial agonists: a new class of antipsychotic. CNS Drugs 18, 251–267. doi:10.2165/00023210-200418040-00005.

Lodge, D.J., Grace, A.A., 2006. The laterodorsal tegmentum is essential for burst firing of ventral tegmental area dopamine neurons. Proc. Natl. Acad. Sci. USA 103, 5167–5172. doi:10.1073/pnas.0510715103.

MacGregor, D.A., Smith, T.E., Prielipp, R.C., Butterworth, J.F., James, R.L., Scuderi, P.E., 2000. Pharmacokinetics of dopamine in healthy male subjects. Anesthesiology 92, 338–346. doi:10.1097/00000542-200002000-00013.

Marshall, L., Mathys, C., Ruge, D., de Berker, A.O., Dayan, P., Stephan, K.E., Bestmann, S., 2016. Pharmacological fingerprints of contextual uncertainty. PLoS Biol. 14, e1002575. doi:10.1371/journal.pbio.1002575.

Mathys, C., Daunizeau, J., Friston, K.J., Stephan, K.E., 2011. A Bayesian foundation for individual learning under uncertainty. Front. Hum. Neurosci. 5, 39. doi:10.3389/fnhum.2011.00039.

Mathys, C.D., Lomakina, E.I., Daunizeau, J., Iglesias, S., Brodersen, K.H., Friston, K.J., Stephan, K.E., 2014. Uncertainty in perception and the Hierarchical Gaussian Filter. Front. Hum. Neurosci. 8, 825. doi:10.3389/fnhum.2014.00825.

Mena-Segovia, J., Winn, P., Bolam, J.P., 2008. Cholinergic modulation of midbrain dopaminergic systems. Brain Res. Rev. 58, 265–271. doi:10.1016/j.brainresrev.2008.02.003.

Mesulam, M.M., Mufson, E.J., Wainer, B.H., Levey, A.I., 1983. Central cholinergic pathways in the rat: an overview based on an alternative nomenclature (Ch1-Ch6). Neuroscience 10, 1185–1201. doi:10.1016/0306-4522(83)90108-2.

Miller, A.D., Blaha, C.D., 2005. Midbrain muscarinic receptor mechanisms underlying regulation of mesoaccumbens and nigrostriatal dopaminergic transmission in the rat. Eur. J. Neurosci. 21, 1837–1846. doi:10.1111/j.1460-9568.2005.04017.x.

Montague, P.R., Hyman, S.E., Cohen, J.D., 2004. Computational roles for dopamine in behavioural control. Nature 431, 760–767. doi:10.1038/nature03015.

Moran, R.J., Campo, P., Symmonds, M., Stephan, K.E., Dolan, R.J., Friston, K.J., 2013. Free energy, precision and learning: the role of cholinergic neuromodulation. J. Neurosci. 33, 8227–8236. doi:10.1523/JNEUROSCI.4255-12.2013.

Naidich, T.P., Duvernoy, H.M., Delman, B.N., Sorensen, A.G., Kollias, S.S., Haacke, E.M., 2009. Duvernoy's Atlas of the Human Brain Stem and Cerebellum: High-Field MRI, Surface Anatomy, Internal Structure, Vascularization and 3 D Sectional Anatomy. Springer Verlag.

Nakahara, H., 2014. Multiplexing signals in reinforcement learning with internal models and dopamine. Curr. Opin. Neurobiol. 25, 123–129. doi:10.1016/j.conb.2014.01.001.

Naude, J., Tolu, S., Dongelmans, M., Torquet, N., Valverde, S., Rodriguez, G., Pons, S., Maskos, U., Mourot, A., Marti, F., Faure, P., 2016. Nicotinic receptors in the ventral tegmental area promote uncertainty-seeking. Nat. Neurosci. 19, 471–478. doi:10.1038/nn.4223.

Newman, E.L., Gupta, K., Climer, J.R., Monaghan, C.K., Hasselmo, M.E., 2012. Cholinergic modulation of cognitive processing: insights drawn from computational models. Front. Behav. Neurosci. 6, 24. doi:10.3389/fnbeh.2012.00024.

Noetzli, M., Eap, C.B., 2013. Pharmacodynamic, pharmacokinetic and pharmacogenetic

aspects of drugs used in the treatment of Alzheimer's disease. Clin. Pharmacokinet. 52, 225–241. doi:10.1007/s40262-013-0038-9.
Oakman, S.A., Faris, P.L., Kerr, P.E., Cozzari, C., Hartman, B.K., 1995. Distribution of pontomesencephalic cholinergic neurons projecting to substantia nigra differs significantly from those projecting to ventral tegmental area. J. Neurosci. 15, 5859–5869.
Okada, K., Nakamura, K., Kobayashi, Y., 2011. A neural correlate of predicted and actual reward-value information in monkey pedunculopontine tegmental and dorsal raphe nucleus during saccade tasks. Neural Plast. 2011, 579840. doi:10.1155/2011/579840.
Pahapill, P.A., Lozano, A.M., 2000. The pedunculopontine nucleus and Parkinson's disease. Brain 123 (Pt 9), 1767–1783. doi:10.1093/brain/123.9.1767.
Parr, T., Friston, K.J., 2017. Uncertainty, epistemics and active inference. J. R. Soc. Interface 14, 20170376. doi:10.1098/rsif.2017.0376.
Payzan-LeNestour, E., Dunne, S., Bossaerts, P., O'Doherty, J.P., 2013. The neural representation of unexpected uncertainty during value-based decision making. Neuron 79, 191–201. doi:10.1016/j.neuron.2013.04.037.
Pearson-Fuhrhop, K.M., Minton, B., Acevedo, D., Shahbaba, B., Cramer, S.C., 2013. Genetic variation in the human brain dopamine system influences motor learning and its modulation by L-Dopa. PLoS One 8, e61197. doi:10.1371/journal.pone.0061197.
Penny, W.D., Stephan, K.E., Daunizeau, J., Rosa, M.J., Friston, K.J., Schofield, T.M., Leff, A.P., 2010. Comparing families of dynamic causal models. PLoS Comput. Biol. 6, e1000709. doi:10.1371/journal.pcbi.1000709.
Pessiglione, M., Seymour, B., Flandin, G., Dolan, R.J., Frith, C.D., 2006. Dopamine-dependent prediction errors underpin reward-seeking behaviour in humans. Nature 442, 1042–1045. doi:10.1038/nature05051.
Piray, P., den Ouden, H.E.M., van der Schaaf, M.E., Toni, I., Cools, R., 2017. Dopaminergic modulation of the functional ventrodorsal architecture of the human striatum. Cereb. Cortex 27, 485–495. doi:10.1093/cercor/bhv243.
Rao, R.P., Ballard, D.H., 1999. Predictive coding in the visual cortex: a functional interpretation of some extra-classical receptive-field effects. Nat. Neurosci. 2, 79–87. doi:10.1038/4580.
Rigoux, L., Stephan, K.E., Friston, K.J., Daunizeau, J., 2014. Bayesian model selection for group studies – revisited. Neuroimage 84, 971–985. doi:10.1016/j.neuroimage.2013.08.065.
Roden, D.M., George Jr., A.L., 2002. The genetic basis of variability in drug responses. Nat. Rev. Drug Discov. 1, 37–44. doi:10.1038/nrd705.
Roeper, J., 2013. Dissecting the diversity of midbrain dopamine neurons. Trends Neurosci. 36, 336–342. doi:10.1016/j.tins.2013.03.003.
Rosenzweig, P., Canal, M., Patat, A., Bergougnan, L., Zieleniuk, I., Bianchetti, G., 2002. A review of the pharmacokinetics, tolerability and pharmacodynamics of amisulpride in healthy volunteers. Hum. Psychopharmacol. 17, 1–13. doi:10.1002/hup.320.
Schilstrom, B., Ivanov, V.B., Wiker, C., Svensson, T.H., 2007. Galantamine enhances dopaminergic neurotransmission in vivo via allosteric potentiation of nicotinic acetylcholine receptors. Neuropsychopharmacology 32, 43–53. doi:10.1038/sj.npp.1301087.
Schoemaker, H., Claustre, Y., Fage, D., Rouquier, L., Chergui, K., Curet, O., Oblin, A., Gonon, F., Carter, C., Benavides, J., Scatton, B., 1997. Neurochemical characteristics of amisulpride, an atypical dopamine D2/D3 receptor antagonist with both presynaptic and limbic selectivity. J. Pharmacol. Exp. Ther. 280, 83–97.
Schultz, W., 2012. Updating dopamine reward signals. Curr. Opin. Neurobiol. 23, 229–238. doi:10.1016/j.conb.2012.11.012.
Schultz, W., Dayan, P., Montague, P.R., 1997. A neural substrate of prediction and reward. Science 275, 1593–1599. doi:10.1126/science.275.5306.1593.
Schwartenbeck, P., FitzGerald, T.H., Mathys, C., Dolan, R., Friston, K., 2015. The dopaminergic midbrain encodes the expected certainty about desired outcomes. Cereb. Cortex 25, 3434–3445. doi:10.1093/cercor/bhu159.
Stalnaker, T.A., Howard, J.D., Takahashi, Y.K., Gershman, S.J., Kahnt, T., Schoenbaum, G., 2019. Dopamine neuron ensembles signal the content of sensory prediction errors. Elife 8. doi:10.7554/eLife.49315.
Stephan, K.E., Baldeweg, T., Friston, K.J., 2006. Synaptic plasticity and dysconnection in schizophrenia. Biol. Psychiatry 59, 929–939. doi:10.1016/j.biopsych.2005.10.005.
Stephan, K.E., Iglesias, S., Heinzle, J., Diaconescu, A.O., 2015. Translational perspectives for computational neuroimaging. Neuron 87, 716–732. doi:10.1016/j.neuron.2015.07.008.
Stephan, K.E., Penny, W.D., Daunizeau, J., Moran, R.J., Friston, K.J., 2009. Bayesian model selection for group studies. Neuroimage 46, 1004–1017. doi:10.1016/j.neuroimage.2009.03.025.
Takahashi, Y.K., Batchelor, H.M., Liu, B., Khanna, A., Morales, M., Schoenbaum, G., 2017. Dopamine neurons respond to errors in the prediction of sensory features of expected rewards. Neuron 95, 1395–1405. doi:10.1016/j.neuron.2017.08.025, e1393.
Threlfell, S., Lalic, T., Platt, N.J., Jennings, K.A., Deisseroth, K., Cragg, S.J., 2012. Striatal dopamine release is triggered by synchronized activity in cholinergic interneurons. Neuron 75, 58–64. doi:10.1016/j.neuron.2012.04.038.
van den Bergh, D., van Doorn, J., Marsman, M., Draws, T., van Kesteren, E.-J., Derks, K., Dablander, F., Gronau, Q.F., Kucharský, Š., Gupta, A.R.K.N., Sarafoglou, A., Voelkel, J.G., Stefan, A., Ly, A., Hinne, M., Matzke, D., Wagenmakers, E.-J., 2020. A tutorial on conducting and interpreting a Bayesian ANOVA in JASP. L'Année Psychol. 120, 73–96. doi:10.3917/anpsy1.201.0073.
van der Schaaf, M.E., van Schouwenburg, M.R., Geurts, D.E., Schellekens, A.F., Buitelaar, J.K., Verkes, R.J., Cools, R., 2014. Establishing the dopamine dependency of human striatal signals during reward and punishment reversal learning. Cereb. Cortex 24, 633–642. doi:10.1093/cercor/bhs344.
van Doorn, J., van den Bergh, D., Böhm, U., Dablander, F., Derks, K., Draws, T., Etz, A., Evans, N.J., Gronau, Q.F., Haaf, J.M., 2020. The JASP guidelines for conducting and reporting a Bayesian analysis. Psychon. Bull. Rev. 1–14.
Vaucher, E., Hamel, E., 1995. Cholinergic basal forebrain neurons project to cortical microvessels in the rat: electron microscopic study with anterogradely transported Phaseolus vulgaris leucoagglutinin and choline acetyltransferase immunocytochemistry. J. Neurosci. 15, 7427–7441.
Vilaró, M.T., Palacios, J., Mengod, G., 1990. Localization of m5 muscarinic receptor mRNA in rat brain examined by in situ hybridization histochemistry. Neurosci. Lett. 114, 154–159. doi:10.1016/0304-3940(90)90064-g.
und von Bohlen, Halbach, O, Dermietzel, R., 2006. Neurotransmitters and Neuromodulators: Handbook of Receptors and Biological Effects Wiley, com.
Vossel, S., Bauer, M., Mathys, C., Adams, R.A., Dolan, R.J., Stephan, K.E., Friston, K.J., 2014. Cholinergic stimulation enhances Bayesian belief updating in the deployment of spatial attention. J. Neurosci. 34, 15735–15742. doi:10.1523/JNEUROSCI.0091-14.2014.
Wagenmakers, E.-J., Love, J., Marsman, M., Jamil, T., Ly, A., Verhagen, J., Selker, R., Gronau, Q.F., Dropmann, D., Boutin, B., Meerhoff, F., Knight, P., Raj, A., van Kesteren, E.-J., van Doorn, J., Šmíra, M., Epskamp, S., Etz, A., Matzke, D., de Jong, T., van den Bergh, D., Sarafoglou, A., Steingroever, H., Derks, K., Rouder, J.N., Morey, R.D., 2018a. Bayesian inference for psychology. Part II: example applications with JASP. Psychon. Bull. Rev. 25, 58–76. doi:10.3758/s13423-017-1323-7.
Wagenmakers, E.-J., Marsman, M., Jamil, T., Ly, A., Verhagen, J., Love, J., Selker, R., Gronau, Q.F., Šmíra, M., Epskamp, S., Matzke, D., Rouder, J.N., Morey, R.D., 2018b. Bayesian inference for psychology. Part I: theoretical advantages and practical ramifications. Psychon. Bull. Rev. 25, 35–57. doi:10.3758/s13423-017-1343-3.
Wise, R.A., 2004. Dopamine, learning and motivation. Nat. Rev. Neurosci. 5, 483–494. doi:10.1038/nrn1406.
Ye, M., Hayar, A., Strotman, B., Garcia-Rill, E., 2010. Cholinergic modulation of fast inhibitory and excitatory transmission to pedunculopontine thalamic projecting neurons. J. Neurophysiol. 103, 2417–2432. doi:10.1152/jn.01143.2009.
Yeomans, J., Forster, G., Blaha, C., 2001. M5 muscarinic receptors are needed for slow activation of dopamine neurons and for rewarding brain stimulation. Life Sci. 68, 2449–2456. doi:10.1016/s0024-3205(01)01038-4.
Young, A.M., Ahier, R.G., Upton, R.L., Joseph, M.H., Gray, J.A., 1998. Increased extracellular dopamine in the nucleus accumbens of the rat during associative learning of neutral stimuli. Neuroscience 83, 1175–1183. doi:10.1016/s0306-4522(97)00483-1.
Yu, A.J., Dayan, P., 2005. Uncertainty, neuromodulation, and attention. Neuron 46, 681–692. doi:10.1016/j.neuron.2005.04.026.
Zaborszky, L., Duque, A., 2003. Sleep-wake mechanisms and basal forebrain circuitry. Front. Biosci. 8, d1146–d1169. doi:10.2741/1112.
Zaborszky, L., Hoemke, L., Mohlberg, H., Schleicher, A., Amunts, K., Zilles, K., 2008. Stereotaxic probabilistic maps of the magnocellular cell groups in human basal forebrain. Neuroimage 42, 1127–1141. doi:10.1016/j.neuroimage.2008.05.055.
Zhou, F.M., Wilson, C., Dani, J.A., 2003. Muscarinic and nicotinic cholinergic mechanisms in the mesostriatal dopamine systems. Neuroscientist 9, 23–36. doi:10.1177/1073858402239588.
Zoli, M., Jansson, A., Sykova, E., Agnati, L.F., Fuxe, K., 1999. Volume transmission in the CNS and its relevance for neuropsychopharmacology. Trends Pharmacol. Sci 20, 142–150. doi:10.1016/s0165-6147(99)01343-7.
Zrinzo, L., Zrinzo, L.V., Massey, L.A., Thornton, J., Parkes, H.G., White, M., Yousry, T.A., Strand, C., Revesz, T., Limousin, P., Hariz, M.I., Holton, J.L., 2011. Targeting of the pedunculopontine nucleus by an MRI-guided approach: a cadaver study. J. Neural Transm. 118, 1487–1495. doi:10.1007/s00702-011-0639-0.
Zubieta, J.K., Frey, K.A., 1993. Autoradiographic mapping of M3 muscarinic receptors in the rat brain. J. Pharmacol. Exp. Ther. 264, 415–422.